Editors' Suggestion

Theory of bubble tips in strong viscous flows

Jens Eggers
School of Mathematics, University of Bristol, Fry Building, Woodland Road, Bristol BS8 1UG, United Kingdom

(Received 3 January 2021; accepted 29 March 2021; published 26 April 2021)

A free surface, placed in a strong viscous flow (such that viscous forces overwhelm surface tension), often develops ends with very sharp tips. In Courrech du Pont and Eggers [Proc. Natl. Acad. U. S. A. **117**, 32238 (2020)] we have shown that the axisymmetric shape of the ends, nondimensionalized by the tip curvature, is governed by a universal similarity solution. The shape of the similarity solution is close to a cone, but whose slope varies with the square root of the logarithmic distance from the tip. Here we develop the calculation of the tip similarity solution to next order, using which we demonstrate matching to previous slender-body analyses, which fail near the tip. This allows us to resolve the long-standing problem, first raised by G. I. Taylor, of finding the global solution of a bubble in a strong hyperbolic flow. We also calculate the tip curvature quantitatively, beyond the scaling behavior of the leading-order solution. Our results are shown to agree in detail with full numerical simulations of the Stokes equation.

DOI: 10.1103/PhysRevFluids.6.044005

I. INTRODUCTION

There exist a wide range of applications, for example in the chemical industry [1,2], in which bubbles are deformed by a variety of flows. G. I. Taylor [3] proposed to study the problem of deformation systematically by placing drops or bubbles in a simple extensional or shear flow, assuming low Reynolds number; another example is a bubble rising in a viscous fluid [5]. In all of these cases, if the flow is sufficiently strong, and if the inner viscosity is much smaller than the outer viscosity, the drop is elongated and terminates in an almost conical end whose tip is so sharp that its radius of curvature is difficult to measure, as seen on the left of Fig. 1.

Later Taylor [6] developed an approximate theory using the slenderness of the drop, from which he calculated the shape of the drop as well as its limits of stability. The same system has subsequently been much studied theoretically [7–10], numerically [11,12], and experimentally [13,14]. In particular, it was shown that Taylor's theory can be derived in a systematic expansion for large capillary number, which measures the strength of the flow in units of the capillary speed γ/η; here γ is the surface tension and η the shear viscosity. An analysis of Taylor's theory near the tip position $z_{\rm tip}$ [15] leads to the conical shape

$$h = \frac{z_{\rm tip} - z}{2v_z^{(\rm ext)}}, \tag{1}$$

where the external axial velocity is taken in units of the capillary speed.

However, Taylor [6] noticed and Buckmaster [7] confirmed that cone-shaped bubble ends, predicted by the leading-order slender-body theory, cannot be a solution of the full Stokes equation: the theory breaks down near the ends. This is not surprising, since the drop shape at the very end does not remain slender. Rather, the difficulty of dealing with an object's ends is a problem shared with the myriad of other applications of slender body theory, for example in Stokes flow around

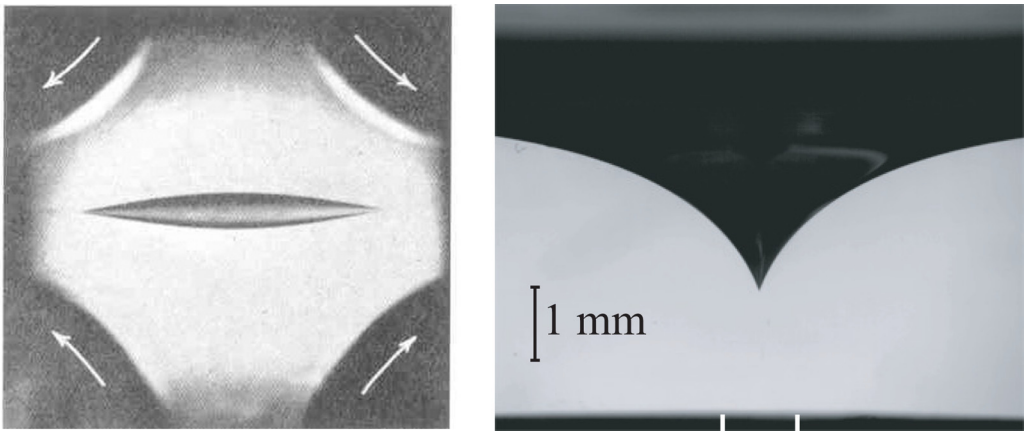

FIG. 1. On the left, a drop of low-viscosity fluid is stretched in Taylor's "four-roller" machine [3]. Very sharp tips form at the ends, while the drop remains stable. On the right, the air-liquid surface of a container draining from a whole in the bottom [4] (silicone oil, $\eta = 60\,\mathrm{Pa\,s}$ and flow rate $q = 3.9\,10^{-3}\,\mathrm{ml/s}$). In both experimental images the ends are in fact not strictly conical but have an opening angle which depends on the scale of observation.

particles [16], aerodynamics [17], or ship hydrodynamics [18,19]. Therefore, it is of fundamental interest to develop a uniformly valid description of slender objects, and to demonstrate how it fits into the classical theories of the bulk of the object.

To improve on Taylor's theory, and to investigate its validity, the slender-body theory of drops was extended to second order [7,9], revealing a logarithmic divergence as the tip is approached. This only highlights the difficulty of describing the tip. First, it leaves open the question of the size of the tips, or even whether the radius of curvature vanishes or remains finite. Second, the logarithmic dependence has lead to the incorrect conclusion that Taylor's leading-order theory fails only on a scale exponentially small in the capillary number [7]. On the contrary, we find that the slope of the interface in fact depends logarithmically on the distance from the tip, as illustrated in Figs. 2(b)–2(f).

On the top, we see the entire bubble as calculated numerically in [15], using a boundary integral method (described in more detail below), which solves directly for the stationary shape. The bubble is deformed by an external extensional flow as on the left of Fig. 1, such that it has been stretched out to a total length of $2\ell = 9.952$, in units of the undeformed drop radius. In the five panels below in Fig. 2, we show the left-hand corner of the bubble with successively higher magnification.

In the top left panel, we show a region of unit size from the tip, which is compared to the asymptotic form of Taylor's theory (1) (dashed line), where the tip position z_{tip} was taken from the simulation; good agreement is found. For each successive panel, the region shown is smaller by $1/100$, giving an increasingly magnified view of the corner. While the dashed line remains invariant, the slope of the actual interface increases. The fifth and last panel finally shows the corner on the scale of the size of the tip.

This illustrates that when measuring the slope of conical ends, as seen for example in Fig. 1, the result will depend on the scale of resolution at which the end is observed, somewhat similar to the apparent contact angle of a spreading drop [20].

More recently, the pointed ends have turned out to be the most interesting part of the solution, owing to the 'tipstreaming' phenomenon noticed by Taylor [3]. Under flow conditions which are not yet understood and often aided by surfactants, thin jets are ejected from the tip. This flow state has been exploited systematically in microfluidics [21,22], where tipstreaming can be provoked under controlled flow conditions. The subsequent Rayleigh decay of jets can produce drops of

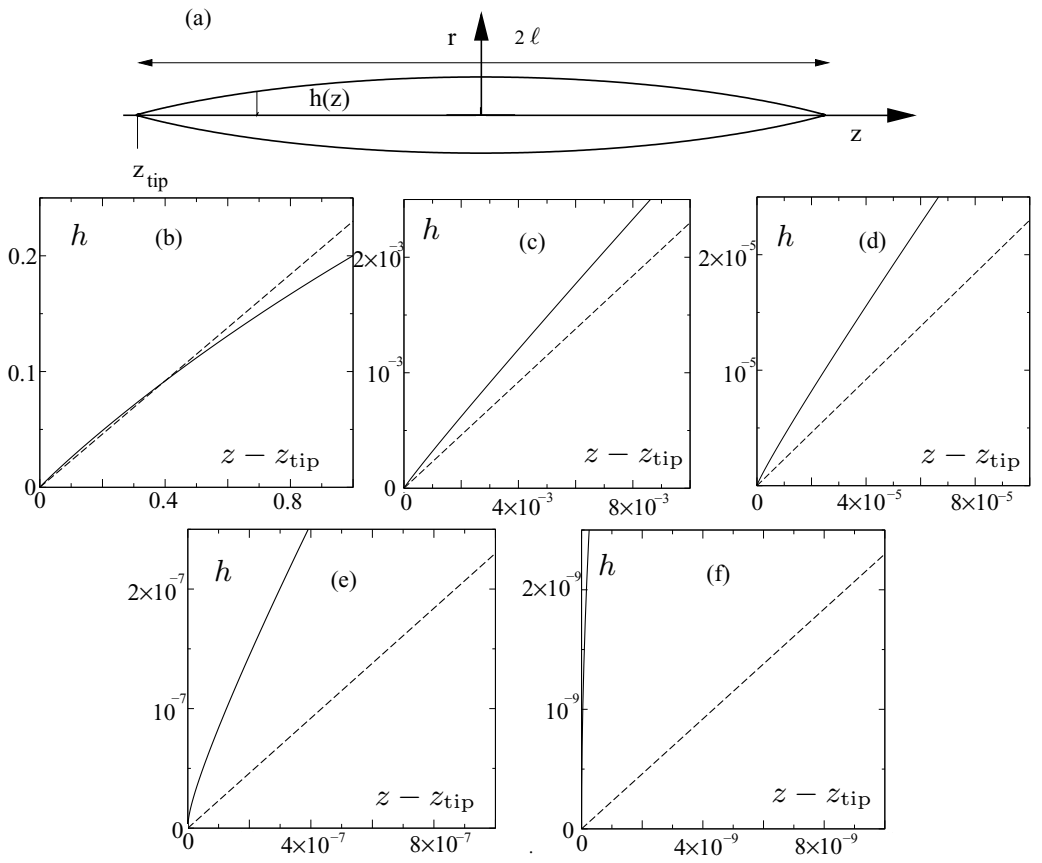

FIG. 2. On the top, the shape $h(z)$ of an inviscid drop (or bubble) in the flow (3) at $\mathrm{Ca} = 0.4393$, as computed with the boundary integral code developed in [15]: (a). The curvature at the tip is $\kappa_m = 2.54 \times 10^8$ in units of the unperturbed drop radius R_d; z_{tip} is the position of the left tip, and the drop half-length is $\ell = 4.976$ in the same units. Panels (b)–(f) on the bottom show the corner of the drop (solid line) compared with the conical approximation (1) of Taylor's theory (dashed line). Starting from the upper left, for each panel we have zoomed in by another factor of $1/100$; the local slope of the interface is seen to increase at each step.

micron size and perhaps below [22]. The tipstreaming phenomenon has been addressed numerically [23,24] and using slender body theory [25,26]; however the latter description suffers from the same shortcomings as Taylor's [6] original work.

Another geometry that has frequently been used to study conical tips as well as the ejection of jets is that of the selective withdrawal experiment [4,15,27,28]. In this setup (see Fig. 1, right), one fluid is extracted from near the interface between two fluids. Recently we have demonstrated [29] that the tip similarity solution agrees well with the tip region of the selective withdrawal experiment. However, selective withdrawal differs from the drop problem in that the geometry does not remain slender far from the tip, and the interface slope in fact becomes large, as seen on the right of Fig. 1. As a result, the theoretical description remains confined to a small region around the tip, as we are not able to describe the transition toward the bulk of the flow, as we will do in the present paper for the drop problem.

The (nearly) axisymmetric tip singularities to be investigated here complete our understanding of the possible singularities of stationary free surfaces in viscous flows. Tips are superficially similar to cusp singularities [30–33], but which form a *line* in three dimensions. Cusps are described locally

by a *two-dimensional* flow in the plane perpendicular to the cusp line, while our new solutions are fully three-dimensional. Complex variable methods have provided multiple examples for global flow solutions with cusps [31,34,35]; now our second-order expansion will allow us to construct global solutions with three-dimensional tips.

Numerical analysis of bubbles in a variety of flows, as well as of the interface in the selective withdrawal geometry [15], indicates that the shape $h(z)$ near the tip is a universal similarity solution of the form [cf. Fig. 2(a)]

$$h(z) = \kappa_m^{-1} H(\zeta), \tag{2}$$

where $\zeta = (z - z_{\rm tip})\kappa_m$ measures the distance from the tip in units of the tip curvature. Here κ_m is the twice the three-dimensional mean curvature at the tip, and $H(\zeta)$ is expected to be a universal function, independent of the outer flow characteristics, or the geometry. In the particular case of a bubble of length 2ℓ [cf. Fig. 2(a)] we will consider the tip located at $z_{\rm tip} = -\ell$.

In the present paper, we calculate $H(\zeta)$ theoretically, and demonstrate that the similarity solution matches onto previous slender-body solutions, to second order in the slenderness parameter. While the tip region is universal, the overall bubble shape depends on the external driving. Following Taylor [3,6], we consider a bubble in the simplest external extensional flow:

$$v_z^{(\rm ext)} = Gz, \quad v_r^{(\rm ext)} = -\frac{G}{2} r, \quad p^{(\rm ext)} = 0, \tag{3}$$

where G is the local rate of extension. Conventionally, the capillary number is defined as $\mathrm{Ca} = GR_d\eta/\gamma$, where R_d is the unperturbed drop radius. For simplicity, we assume that the entire problem is axisymmetric, that the interior of the bubble has vanishing viscosity, and that the Reynolds number of the flow is zero, so Stokes' equation can be used. Since the outer flow sets a characteristic velocity scale, we expect that on the small scale, near the tip, the Reynolds number will be small. However, the global features of the flow will be different if the external flow is not axisymmetric [10], or the Reynolds number is not small [9].

Our theoretical analysis is based directly on the boundary integral equations [11,36], which are an exact formulation of the Stokes equation, and particularly suited to describing free surface motion, as the integration is over the free surface only, without having to describe the entire flow. As far as we are aware, boundary integral equations have chiefly been used as a numerical tool, since they involve integration over an unknown surface in three dimensions, making them awkward to handle in analytical terms. The key insight here is that the interface is almost conical, with an opening angle which varies on a logarithmic scale only. This allows us to reformulate the equations as a local problem on a logarithmic scale, where locally the surface is conical, so integrals can be evaluated analytically.

In the next section, we develop the equations for the tip region, based on the boundary integral equations. Since the interface slope decreases with the distance from the tip, we are able to develop a perturbative approach, valid in the far field of the similarity solution $H(\zeta)$, We solve the resulting dynamical equation for the slope to leading order, expanding on the brief account in [29], and add a "back-of-the-envelope"-type derivation, based on physical insight and previous exact flow solutions.

In Sec. III we develop the asymptotics to next order, crucial for matching to the bubble, proving the consistency of the approach, and significantly improving the accuracy of our predictions. In the following Sec. IV we briefly recall Buckmaster's [7] slender body expansion, and calculate the surface profiles and the velocity profiles to next-to-leading order in the slenderness parameter. Then, in Sec. V we are able to match the inner similarity solution with the slender body expansion to second order, providing us with a uniformly valid composite solution for the entire drop. As a by-product, we calculate the tip curvature as function of the capillary number beyond the scaling prediction of [29]. In the final discussion we mention possibilities for future investigations.

II. SIMILARITY THEORY

A. Boundary integral equations

Our starting point is the boundary integral equation [37] for the velocity $\mathbf{v}$ at a point $\mathbf{x}_1$ on the surface:

$$\frac{\mathbf{v}(\mathbf{x}_1)}{2} = \mathbf{v}^{(\mathrm{ext})}(\mathbf{x}_1) - \int_S \kappa \mathbf{J}\cdot\mathbf{n}\, d\sigma_2 - \int_S \mathbf{v}\cdot\mathbf{K}\cdot\mathbf{n}\, d\sigma_2, \tag{4}$$

where, putting $\mathbf{r} = \mathbf{x}_1 - \mathbf{x}_2$,

$$J_{ij}(\mathbf{r}) = \frac{1}{8\pi}\left[\frac{\delta_{ij}}{r} + \frac{r_i r_j}{r^3}\right], \quad K_{ijk}(\mathbf{r}) = -\frac{3}{4\pi}\frac{r_i r_j r_k}{r^5}. \tag{5}$$

We have written (4) for the special case of vanishing viscosity inside the drop; the surface integrals are over an entire closed surface, e.g. over the drop. Velocities have been written in units of the capillary speed γ/η, so neither parameter appears. The idea of (4) is to write the action of surface tension as a superposition of point forces over the free surface, which corresponds to the first integral on the right of (4). The strength of each point force is proportional to (twice) the mean curvature of the interface κ, $\mathbf{n}$ is the outward unit normal, and J_{ij} is the free-space Stokeslet, i.e., the velocity field generated by a point force located at $\mathbf{x}_2$. The second integral on the right of (4) accounts for the mismatch in stress produced by the jump in viscosity across the interface; K_{ijk} is the free-space stresslet, the distribution of stress generated by a point force. The term $\mathbf{v}^{(\mathrm{ext})}(\mathbf{x}_1)$ is the externally imposed velocity field, for example, (3). In this paper, we are concerned exclusively with steady states. In the numerical investigation [15], a steady state is found directly by requiring that the free surface be a streamline of the flow, as described by (4), and the volume of the drop is constrained to a given value. The resulting equations are solved using Newton's method, which is much more efficient than solving the time-dependent problem and waiting for the shape to converge toward a steady state.

It can be advantageous, both numerically and for the analytical treatment below, to remove the leading-order singularities in the K-kernels. To that end we use the exact relation [36]

$$\int_S \mathbf{K}\cdot\mathbf{n}\, d\sigma_2 = \frac{\mathbf{I}}{2}, \tag{6}$$

where $\mathbf{I}$ is the identity matrix. This allows us to write (4) in the form

$$\mathbf{v}(\mathbf{x}_1) = \mathbf{v}^{(\mathrm{ext})}(\mathbf{x}_1) + \mathbf{v}^{(J)}(\mathbf{x}_1) - \int_S [\mathbf{v}(\mathbf{x}_2) - \mathbf{v}(\mathbf{x}_1)]\cdot\mathbf{K}\cdot\mathbf{n}\, d\sigma_2, \tag{7}$$

where

$$\mathbf{v}^{(J)}(\mathbf{x}_1) = -\int_S \kappa(\mathbf{x}_2)\mathbf{J}\cdot\mathbf{n}\, d\sigma_2. \tag{8}$$

Since the surface S is axisymmetric, we can perform the integration over the angle, which can be done analytically, leading to elliptic integrals [36]. As a result, the three-dimensional Cartesian vector Eqs. (7) and (8) become two-dimensional expressions for the axial and radial components of a cylindrical coordinate system (z, r) alone. Thus we define, putting $\mathbf{x}_1 = (y_1, 0, z_1)$, $\mathbf{x}_2 = (y_2\cos\theta_2, y_2\sin\theta_2, z_2)$, $\mathbf{e}_z = (0, 0, 1)$, $\mathbf{e}_r(\theta_2) = (\cos\theta_2, \sin\theta_2, 0)$, and $\overline{\mathbf{n}} = (\cos\theta_2, \sin\theta_2, -h'(z_2))$,

$$\mathbf{j} \equiv (j_z, j_r) = y_2 \int_0^{2\pi} [\mathbf{e}_z\cdot\mathbf{J}\cdot\overline{\mathbf{n}}, \mathbf{e}_r(0)\cdot\mathbf{J}\cdot\overline{\mathbf{n}}] d\theta_2. \tag{9}$$

We choose the vector $\overline{\mathbf{n}}$ as not being normalized. Since the line element $dl = \sqrt{1+h'^2}\, dz$, this means we can replace dl by dz in the line integrals below.

Using the two-dimensional matrices

$$\mathbf{k} = \begin{pmatrix} k_1 & k_3 \\ k_2 & k_4 \end{pmatrix}, \quad \mathbf{k}^s = \begin{pmatrix} k_1^s & k_3^s \\ k_2^s & k_4^s \end{pmatrix},$$

corresponding to $\mathbf{v}(\mathbf{x}_2)\cdot\mathbf{K}\cdot\mathbf{n}$ and the subtraction $\mathbf{v}(\mathbf{x}_1)\cdot\mathbf{K}\cdot\mathbf{n}$, respectively, we put

$$k_1 = k_1^s = y_2\mathbf{e}_z\cdot\int_0^{2\pi}(\mathbf{e}_z\cdot\mathbf{K}\cdot\overline{\mathbf{n}})d\theta_2, \tag{10}$$

$$k_2 = k_2^s = k_3^s = y_2\mathbf{e}_r(0)\cdot\int_0^{2\pi}(\mathbf{e}_z\cdot\mathbf{K}\cdot\overline{\mathbf{n}})d\theta_2, \tag{11}$$

$$k_3 = y_2\mathbf{e}_z\cdot\int_0^{2\pi}[\mathbf{e}_r(\theta_2)\cdot\mathbf{K}\cdot\overline{\mathbf{n}}]d\theta_2, \tag{12}$$

$$k_4 = y_2\mathbf{e}_r(0)\cdot\int_0^{2\pi}[\mathbf{e}_r(\theta_2)\cdot\mathbf{K}\cdot\overline{\mathbf{n}}]d\theta_2, \tag{13}$$

$$k_4^s = y_2\mathbf{e}_r(0)\cdot\int_0^{2\pi}[\mathbf{e}_r(0)\cdot\mathbf{K}\cdot\overline{\mathbf{n}}]d\theta_2. \tag{14}$$

With these definitions, (7) becomes

$$\mathbf{v}(z_1) = \mathbf{v}^{(\mathrm{ext})}(z_1) - \int_{-\ell}^{\ell}\kappa(z_2)\mathbf{j}(z_1,z_2)\,dz_2 - \int_{-\ell}^{\ell}\mathbf{k}(z_1,z_2)\cdot\mathbf{v}(z_2)\,dz_2 + \int_{-\ell}^{\ell}\mathbf{k}^s(z_1,z_2)\,dz_2\cdot\mathbf{v}(z_1), \tag{15}$$

where the integrals are now over the axial variable alone.

To study the self-similar tip region, we use (2), writing (15) in units of the tip curvature κ_m, and using the similarity transformation $z = -\ell + \zeta/\kappa_m$; now $\zeta = 0$ corresponds to the left tip of the drop. Setting $\hat{\kappa}(\zeta) = \kappa(z)/\kappa_m$, (15) becomes

$$\mathbf{v}(\zeta_1) = v_{\mathrm{tip}}\mathbf{e}_z - \int_0^{2R}\hat{\kappa}(\zeta_2)\hat{\mathbf{j}}(\zeta_1,\zeta_2)\,d\zeta_2 - \int_0^{2R}\hat{\mathbf{k}}(\zeta_1,\zeta_2)\cdot\mathbf{v}(\zeta_2)\,d\zeta_2 + \int_0^{2R}\hat{\mathbf{k}}^s(\zeta_1,\zeta_2)\,d\zeta_2\cdot\mathbf{v}(\zeta_1), \tag{16}$$

where the hat refers to local variables in units of κ_m. The dimensionless parameter $R = \ell\kappa_m$ measures the tip curvature in units of the drop length. In (16) we also approximated $\mathbf{v}^{(\mathrm{ext})} = v_{\mathrm{tip}}\mathbf{e}_z$, because on a scale of κ_m^{-1}, the external flow can be taken as its value at the tip $z = -\ell$; otherwise (16) is still exact.

Finally, anticipating that the slope near the tip varies on a logarithmic scale, we introduce logarithmic scales $l_1 = \ln\zeta_1$, $l_2 = \ln\zeta_2$, and take everything as functions of l_1 and l_2. As a result, (16) becomes

$$\mathbf{v}(l_1) = v_{\mathrm{tip}}\mathbf{e}_z - \int_{-\infty}^{\ln(2R)}\zeta_2\hat{\kappa}(l_2)\hat{\mathbf{j}}(l_1,l_2)\,dl_2 - \int_{-\infty}^{\ln(2R)}\zeta_2\hat{\mathbf{k}}(l_1,l_2)\cdot\mathbf{v}(l_2)\,dl_2 + \int_{-\infty}^{\ln(2R)}\zeta_2\hat{\mathbf{k}}^s(l_1,l_2)\,dl_2\cdot\mathbf{v}(l_1). \tag{17}$$

Once more, the integration is over the entire drop. Note that the expressions $\zeta_2\hat{\mathbf{k}}(l_1,l_2)$, $\hat{\mathbf{j}}(l_1,l_2)$, and $\zeta_2\hat{\mathbf{k}}^s(l_1,l_2)$ remain invariant under a multiplication of all lengths by a constant. If all integrals were convergent for $R\to\infty$, this parameter could be eliminated and a local solution results. Thus (17) would have a solution for a cone of constant slope, with $\mathbf{v}(l_1)$ a constant. However, we know from [7] that such a solution cannot exist. The reason is that the z-component of the J-integral is logarithmically divergent for $R\to\infty$, as we will see. Thus instead of a strictly conical solution, we

look for a solution of the form

$$H(\zeta) = \zeta s(\ln \zeta), \tag{18}$$

where $s(\ln \zeta) \equiv s(l)$ is the slope of the chord to the tip. The full slope of the interface becomes

$$\frac{dH}{d\zeta} = s(l) + s'(l);$$

we will always use the prime to denote the derivative with respect to the logarithmic variable l. As we will see below, far from the tip the slope becomes small like a power law, so that $s' \ll s$, and one can in fact approximate the slope to leading order as $s(l)$.

As a result of their scale invariance, the kernels $\hat{\mathbf{j}}(l_1, l_2)$ and $\zeta_2 \hat{\mathbf{k}}^s(l_1, l_2)$ can be written in terms of the variables s_1, s_2, s_2', as well as the ratio ζ_2/ζ_1 alone; the dependence on s_2' comes from $\overline{\mathbf{n}}$. Since variables vary on a logarithmic scale, we introduce the logarithmic "distance" $\Delta = l_2 - l_1 = \ln(\zeta_2/\zeta_1)$, and use the self-evident notation $\hat{\mathbf{j}}(l_1, l_2) \equiv \hat{\mathbf{j}}(s_1, s_2, s_2', \Delta)$ and $\zeta_2 \hat{\mathbf{k}}(l_1, l_2) \equiv \zeta_2 \hat{\mathbf{k}}(s_1, s_2, s_2', \Delta)$ for the kernels as functions of the new variables. The curvature, multiplied by ζ_2, is also a function of $s(l)$ and its derivatives alone: $\zeta_2 \hat{\kappa}(l_2) \equiv (\zeta_2 \hat{\kappa})(s_2, s_2', s_2'')$.

B. Back-of-the-envelope calculation

Before we perform a systematic calculation based on the full boundary integral equations, we show how the leading-order result can be obtained with a few simple arguments, using the fact that the approximate slope $s(l)$ becomes small far from the tip. According to the kinematic boundary condition, in a steady state the free surface must be a streamline of the flow, and so $s \approx v_r/v_z$, where v_r and v_z are the radial and axial components of the velocity, respectively, which also vary on the scale l of the logarithmic distance from the tip. In the limit of small slopes, the drop looks like a near-cylindrical cavity inside a viscous fluid, which collapses under the action of surface tension [38]. Assuming a purely radial two-dimensional source flow, balancing surface tension with viscous stresses, the radial velocity is obtained readily (cf. [39], p. 218) as $v_r = -1/2$, so that $v_z \approx -1/(2s)$.

Next we calculate $v_z(l)$, which describes the translation of the interface as a result of the z-component of the hoop stress (the squeezing) produced by surface tension, directed in the positive z-direction, while the contribution v_{tip} from the external flow points in the opposite direction. We guess that a small amount of the same fluid inside the bubble would make little difference to this translation, in which case we can calculate the surface tension contribution to v_z from the J-integral alone, which is the first integral on the right of (17).

For a given logarithmic scale l, we have to add up all the contributions coming from logarithmic scale l_2, lying between the scale of the tip (which is $0 = \ln 1$ in rescaled variables), and the scale of the drop, which is $\ln R$. The contribution from $0 < l_2 < l$ is small, since it effectively comes from a point, of vanishing surface area. In evaluating the contribution from $l < l_2 < \ln R$, we can assume that the interface is approximated locally by a cone, at the tip of which $v_z(l)$ is to be calculated. This situation is very similar to that encountered in the breakup of a fluid drop inside of another fluid [40,41], because the interface on either side of the break point approaches a cone. However, in the present case the slope varies on a logarithmic scale, and v_z has to be taken as the integral of local contributions.

Since the slope is small, the contribution from the mean curvature is dominated by its radial part, and $\zeta_2 \hat{\kappa}(l_2) \approx 1/s_2$. To compute $\hat{j}_z$, we have to integrate the three-dimensional kernel $\mathbf{J} \cdot \mathbf{n}$ of (4) over the circumference of the cone. Since $\mathbf{r}$ in (5) is the vector from the tip of the cone to a point on the surface, $\mathbf{r} \cdot \mathbf{n} = 0$, and only the first term of $\mathbf{J} \cdot \mathbf{n} = \mathbf{n}/(8\pi r)$ contributes. Since the local circumference is $\approx 2\pi s_2 r$, and the z-component of $\mathbf{n}$ is $-s_2$, the result is $\hat{j}_z \approx -s_2^2/4$. Thus $\zeta_2 \hat{\kappa}\, \hat{j}_z \approx -s_2/4$, in agreement with what is found in the two-fluid breakup problem in the limit of

small slopes (cf. [39], p. 181), and we obtain

$$v_z(l) \approx v_{\rm tip} + \int_l^{\ln R} \frac{s_2}{4}\, dl_2.$$

Differentiating with respect to l, we have $v_z' = -s/4$, while from the previous expression for v_z, we obtain $v_z' = s'/(2s^2)$. The resulting equation $s' = -s^3/2$ is solved as $s = 1/\sqrt{l - l_0}$, where l_0 is a constant of integration. This is exactly the result we will obtain more systematically in the following subsection. It shows that the slope is indeed varying slowly as a power law of the logarithmic distance from the tip. Balancing $v_{\rm tip}$ against the contribution from the upper limit of the integral, we obtain an expression for the curvature in terms of the strength of the outer flow. As we will see below, this makes R exponentially large in the *square* of $v_{\rm tip}$.

C. The local approximation: Leading order

The idea for solving the integral Eq. (17) with the ansatz (18) is that on a logarithmic scale, the kernels are peaked as function of the distance Δ. As a result, to some approximation, to be given precisely below, we can write the integral Eq. (17) as a *local* equation for the variables $s(l)$ and $\mathbf{v}(l)$, which we then solve. The constant $v_{\rm tip}$ has to be adjusted such that the R-dependent term in the J-integral cancels, introducing a nonlocal coupling between the behavior near the tip and the outer flow. We aim to solve (17) asymptotically as $l_1 \to \infty$; for a full solution at arbitrary l_1 a numerical treatment is necessary. Considering the integrals one by one, we begin by writing (17) in the form

$$\begin{pmatrix} v_z \\ v_r \end{pmatrix} = \begin{pmatrix} v_{\rm tip} + v_z^{(J)} - K_1 - K_3 \\ v_r^{(J)} - K_2 - K_4 \end{pmatrix}, \tag{19}$$

where $v_r^{(J)}$ and $v_z^{(J)}$ are the two components of the first integral on the right of (17), and K_i corresponds to the contributions coming from the k_i-integrals.

We first perform the calculation to leading order as $l \to \infty$ and $s \to 0$, and calculate corrections to this asymptotic in the following section. We begin with the integral $v_r^{(J)}$, and look at the kernel $\hat{j}_r(s_1, s_2, s_2', \Delta)$, for which

$$\hat{j}_r \approx \begin{cases} \frac{s_1 s_2 (2 - s_2^2) s_2'}{8(1+s_2^2)^{5/2}} e^{-\Delta} & \Delta \to \infty \\ \frac{-(s_2 + s_2^2) s_1 s_2}{4(1+s_1^2)^{3/2}} e^{\Delta} & \Delta \to -\infty, \end{cases} \tag{20}$$

so that j_r converges exponentially in Δ. The result (20) can be found by expanding the final expression for $\hat{j}_r(s_1, s_2, s_2', \Delta)$, containing elliptic integrals, for $\zeta_2/\zeta_1 \to \infty$ and $\zeta_2/\zeta_1 \to 0$, holding s_1, s_2, and s_2' constant; this is done easily with help of an algebraic manipulation package such as MAPLE. Alternatively, the algebra can be simplified by performing the expansions in ζ_2/ζ_1 first for the three-dimensional kernel $\mathbf{J} \cdot \mathbf{n}$ in (8). The angular integration then reduces to integrals over $\cos^i(\theta)$ for $i = 0, 1, 2$, which are trivial.

Now we can let $\ln(2R) \to \infty$, only incurring an exponentially small error of order $1/R$, and obtain

$$v_r^{(J)} \approx -\int_{-\infty}^{\infty} \zeta_2 \hat{k}(l_2) \hat{j}_r(l_1, l_2)\, dl_2. \tag{21}$$

The arguments of $\hat{j}_r(s_1, s_2, s_2', \Delta)$ can be expanded in the form

$$s_2 = s(l_2) = s(l_1) + s'(l_1)\Delta \cdots, \tag{22}$$

where each of the resulting integrals remains convergent. As we will see in more detail below, higher order terms become progressively smaller both since $s' \ll s$ for $l \to \infty$, and since the main contribution to the integral comes from regions $\Delta \approx s$, where s becomes small. Thus to leading

order, we put $s_2 = s_1$ and $s_2' = 0$, so that

$$\hat{j}_r(s_1, s_2, s_2', \Delta) \approx \hat{j}_r(s_1, s_1, 0, \Delta) \equiv \hat{j}_r(s_1, \Delta),$$

which corresponds to the result for a perfect cone with slope $s_1 = s(l_1)$. Expanding the curvature to leading order (the details are given in the next section), we obtain $\zeta_2\hat{\kappa}(l_2) \approx 1/s_2$. Thus expanding s_2 as in (22), we can approximate $\zeta_2\hat{\kappa}(l_2) \approx \zeta_1\hat{\kappa}(l_1)$ and find

$$v_r^{(J)} \approx (\zeta_1\hat{\kappa})(l_1) \int_{-\infty}^{\infty} \hat{j}_r(s_1, \Delta) d\Delta = 0, \tag{23}$$

where we have used that

$$\int_{-\infty}^{\infty} \hat{j}_r(s_1, \Delta) d\Delta = 0. \tag{24}$$

This exact result will be demonstrated in Appendix A, and is confirmed by an expansion for small s, as will be explained in more detail below.

Next we consider the integral $v_z^{(J)}$. Its kernel $\hat{j}_z$ does not decay for large Δ, which is the key to the results of this paper. Instead, expanding for large $|\Delta|$ yields

$$\hat{j}_z \approx \begin{cases} \hat{j}_z^e + \frac{(s_2^2-2)s_2 s_2'}{4(1+s_2^2)^{5/2}} e^{-\Delta} & \Delta \to \infty \\ \frac{-(s_2+s_2')(s_1^2+2)s_2}{4(1+s_1^2)^{3/2}} e^{\Delta} & \Delta \to -\infty, \end{cases} \tag{25}$$

where

$$\hat{j}_z^e \equiv \frac{\big[-\big(s_2+s_2'\big)\big(2+s_2^2\big)+s_2\big]s_2}{4\big(1+s_2^2\big)^{3/2}}. \tag{26}$$

Thus if we split the integral according to

$$v_z^{(J)} = -\int_{-\infty}^{\ln(2R)} \zeta_2\hat{\kappa}(l_2)\hat{j}_z(l_1, l_2)\, dl_2 \approx -\int_{-\infty}^{\infty} \zeta_2\hat{\kappa}\big[\hat{j}_z - H(l_2-l_1)\hat{j}_z^e\big] dl_2 - \int_{l_1}^{\ln(2R)} \zeta_2\hat{\kappa}\hat{j}_z^e\, dl_2, \tag{27}$$

we can take the upper limit to infinity in the first integral on the right, since the integrand converges exponentially according to (25); here H is the Heaviside function.

Now we can approximate the first integral on the right of (27) to leading order using the local approximation $s_2 = s_1$, $s_2' = 0$, starting from (27), which yields

$$\int_{-\infty}^{\infty} \zeta_2\hat{\kappa}\big[\hat{j}_z - H(l_2-l_1)\hat{j}_z^e\big] dl_2 \approx (\hat{\kappa}\zeta)(l_1) \int_{-\infty}^{\infty} \big[\hat{j}_z - H(\Delta)\hat{j}_z^e\big](s_1, \Delta)\, d\Delta \equiv (\hat{\kappa}\zeta)(l_1) I_z(s_1). \tag{28}$$

We will see below that $I_z \propto s^2$, so in the limit of $s \to 0$, the local contribution does not have to be considered. Turning to the second integral on the right of (27), in the limit of small slopes $\hat{j}_z^e \approx -s_2^2/4$ and $\zeta_2\hat{\kappa} = 1/s_2$, and so $\zeta_2\hat{\kappa}\hat{j}_z^e \approx -s_2/4$, and we obtain

$$v_z^{(J)} \approx \frac{1}{4}\int_{l_1}^{\ln(2R)} s(l_2)\, dl_2. \tag{29}$$

Next we consider the K_i-integrals introduced in (19); The kernels $\hat{k}_i$ scale like ζ_2^{-1}, so the $\zeta_2\hat{k}_i$ vary on a logarithmic scale; their behavior is as follows:

$$\zeta_2\hat{k}_1 \approx \begin{cases} -\frac{3s_2 s_2'}{2(1+s_2^2)^{5/2}} + O(e^{-\Delta}) & \Delta \to \infty \\ \frac{3s_2(s_2+s_2')}{2(1+s_2^2)^{5/2}} e^{2\Delta} & \Delta \to -\infty, \end{cases} \quad \zeta_2\hat{k}_2 \approx \begin{cases} -\frac{3s_1 s_2(s_2^3+3s_2^2 s_2'+s2-2s_2')}{4(1+s_2^2)^{7/2}} e^{-\Delta} & \Delta \to \infty \\ \frac{3s_2 s_1(s_2+s_2')}{2(1+s_2^2)^{5/2}} e^{2\Delta} & \Delta \to -\infty, \end{cases} \tag{30}$$

$$\zeta_2\hat{k}_3 \approx \begin{cases} -\frac{3s_2^2 s_2'}{2(1+s_2^2)^{5/2}} + O(e^{-\Delta}) & \Delta \to \infty \\ -\frac{3s_1^2 s_2}{4(1+s_2^2)^{5/2}} e^{2\Delta} & \Delta \to -\infty, \end{cases} \qquad \zeta_2\hat{k}_4 \approx \begin{cases} -\frac{3s_2^2 s_1(s_2^3+2s_2^2 s_2'+s_2-3s_2')}{4(1+s_2^2)^{7/2}} e^{-\Delta} & \Delta \to \infty \\ \frac{3s_1^3 s_2^2}{4(1+s_2^2)^{5/2}} e^{2\Delta} & \Delta \to -\infty, \end{cases} \tag{31}$$

$$\zeta_2\hat{k}_4^s \approx \begin{cases} -\frac{3s_2^3 s_2'}{4(1+s_2^2)^{5/2}} & \Delta \to \infty \\ \frac{3s_1^2 s_1(s_2+s_2')}{2(1+s_1^2)^{5/2}} e^{2\Delta} & \Delta \to -\infty. \end{cases} \tag{32}$$

In other words, for the upper limits of $\hat{k}_1, \hat{k}_3$, and $\hat{k}_4^s$, the asymptotic values $\hat{k}_1^e, \hat{k}_3^e, \hat{k}_4^{s,e}$ need to be subtracted. However, since $s_2' \to 0$ to leading order, there still is algebraic decay, and in each case the integrals remain finite.

Keeping track of algebraic corrections, we identify the entries in (19) as

$$K_1 = \int_{-\infty}^{\infty} \left[\zeta_2\hat{k}_1 - H(\Delta)\hat{k}_1^e\right][v_z(l_2) - v_z(l_1)]\, dl_2 + \int_{l_1}^{\ln(2R)} \hat{k}_1^e v_z(l_2)\, dl_2 - v_z(l_1) \int_{l_1}^{\ln(2R)} \hat{k}_1^e\, dl_2, \tag{33}$$

$$K_2 = \int_{-\infty}^{\infty} \zeta_2\hat{k}_2[v_z(l_2) - v_z(l_1)]dl_2, \tag{34}$$

$$K_3 = \int_{-\infty}^{\infty} \left\{\left[\zeta_2\hat{k}_3 - H(\Delta)\hat{k}_3^e\right]v_r(l_2) - \zeta_2\hat{k}_2 v_r(l_1)\right\}dl_2 + \int_{l_1}^{\ln(2R)} \hat{k}_3^e v_r(l_2)\, dl_2, \tag{35}$$

$$K_4 = \int_{-\infty}^{\infty} \left\{\zeta_2\hat{k}_4 v_r(l_2) - \left[\zeta_2\hat{k}_4^s - H(\Delta)k_4^{s,e}\right]v_r(l_1)\right\}dl_2 - v_r(l_1) \int_{l_1}^{\ln(2R)} k_4^{s,e}\, dl_2. \tag{36}$$

It is easy to perform the integrals to leading order, as all the dominant contributions come from $l_2 \approx l_1$, as we will see in more detail below.

Beginning with the first integral of K_1, and anticipating that the second and third integral of (33) are subdominant, we write $\hat{k}_1(s_1, s_2, s_2', \Delta) \approx \hat{k}_1(s_1, s_1, 0, \Delta)$, and expand the result for small values of s. It is straightforward to confirm that all angular integrals (9)–(14) can be written as a function of a dimensionless combination c, which for a cone of constant slope s can be written as

$$c \equiv \frac{2y_1 y_2}{y_1^2 + y_2^2 + (x_1 - x_2)^2} = \frac{2s^2 e^{\Delta}}{(1+s^2)(1-e^{\Delta})^2 + 2s^2 e^{\Delta}}.$$

In the limit of small s, and putting $\xi = \Delta/s$, this becomes

$$c = \frac{2}{\xi} + O(s).$$

We will confirm in more detail in the next section that to leading order for small s, the main contribution to the integrals comes from the central region of size s. This part of the integral can be captured by expanding in s at constant ξ:

$$\zeta_2\hat{k}_1 = K_1^{(-1)}(\xi)s^{-1} + K_1^{(0)}(\xi) + \cdots, \tag{37}$$

where $K_1^{(-1)}(\xi)$ is an even function in ξ, and the remaining terms alternate between odd and even. Expanding the velocity according to

$$v_z(l_2) = v_z(l_1) + v_z'\Delta + O(\Delta)^2, \tag{38}$$

the leading contribution is $v_z(l_2) - v_z(l_1) \approx v_z'\Delta$. As a result, the first nonvanishing contribution to the first integral in (33) is of order

$$K_1 \approx \int_{-\infty}^{\infty} \zeta_2 k_1(s_1, \Delta)\Delta d\Delta = O(s^2), \tag{39}$$

which will turn out to be of lower order than the contribution from $v_z^{(J)}$, and thus can be neglected at leading order.

Next, the leading contribution to K_2 is

$$K_2 \approx \int_{-\infty}^{\infty} \zeta_2 k_2 \Delta\, d\Delta = v_z' s \int_{-\infty}^{\infty} \xi K_2^{(-1)}\, d\xi + O(s^2) = -v_z' \frac{s}{2} + O(s^3), \tag{40}$$

using that

$$\zeta_2 k_2 = K_2^{(-1)}(\xi) s^{-1} + K_2^{(0)}(\xi) + \cdots,$$

where $K_2^{(-1)}(\xi)$ is odd, and we show in Appendix A that

$$\int_{-\infty}^{\infty} \xi K_2^{(-1)}(\xi)\, d\xi = -\frac{1}{2}. \tag{41}$$

In K_3, the second, nonlocal integral is again subdominant, and since $v_r(l_2) - v_r(l_1) = O(\Delta)$ the leading contribution comes from $v_r(l_2) \approx v_r(l_1)$. As a result,

$$K_3 \approx v_r(l_1) \int_{-\infty}^{\infty} \zeta_2(k_3 - k_2)\, d\Delta = v_r s \int_{-\infty}^{\infty} K_3^0\, d\xi + O(s^2) = v_r \frac{s}{2} + O(s^2), \tag{42}$$

where

$$\zeta_2(k_3 - k_2) = K_3^{(-1)}(\xi) s^{-1} + K_3^{(0)}(\xi) + \cdots,$$

and $K_3^{(-1)}(\xi)$ is odd, so only $K_3^{(0)}(\xi)$ contributes at leading order.

Finally, to calculate K_4 we once more approximate $v_r(l_2) \approx v_r(l_1)$ and consider only local contributions. The local expansion of the kernel is

$$\zeta_2\big(k_4 - k_4^s\big) = K_4^{(-1)}(\xi) s^{-1} + K_4^{(0)}(\xi) + K_4^{(1)}(\xi) s + \cdots,$$

where $K_4^{(-1)}(\xi)$ and $K_4^{(1)}(\xi)$ are odd. Thus

$$K_4 \approx v_r(l_1) \int_{-\infty}^{\infty} \zeta_2\big(k_4 - k_4^s\big)\, d\Delta = v_r\left(\int_{-\infty}^{\infty} K_4^{(-1)}\, d\xi + s^2 \int_{-\infty}^{\infty} K_4^{(1)}\, d\xi\right) = \left(-1 + \frac{s^2}{4}\right) v_r. \tag{43}$$

Inserting this into (19), to leading order we obtain the system

$$v_z = v_{\text{tip}} + \frac{1}{4}\int_l^{\ln(2R)} s(l_2)\, dl_2 + O(s), \quad 0 = \frac{s}{2} v_z' - \frac{s^2}{4} v_r + O(s^4), \tag{44}$$

which, apart from the integral, is the desired local formulation of the boundary integral equations. The consistency of our calculation will be confirmed in the next section. From the kinematic boundary condition, we have $dH/d\zeta = s + s' \approx s = v_r/v_z$. Differentiating the first equation of (44) we get $v_z' = -s/4$ to leading order, and so from the second equation of (44) $v_r = -1/2$, consistent with the anticipated result of the preceding subsection.

Thus exactly as in Sec. II B we find $s'(l) = -s^3/2$. The solution of this equation is $s = (l - l_0)^{-1/2}$, so we finally have

$$s = (l - l_0)^{-1/2}, \quad v_r = -\frac{1}{2}, \quad v_z = -\frac{\sqrt{l - l_0}}{2}, \tag{45}$$

and the asymptotic shape of the similarity profile (18) is

$$H(\zeta) = \frac{\zeta}{\sqrt{\ln(\zeta) - l_0}}. \tag{46}$$

The constant of integration l_0 is to be determined from matching to the full integral formulation for the similarity solution of the tip region.

To obtain the similarity profile $H(\zeta)$ for any value of ζ, we have to solve the full integral equation (16), written in inner variables. In order to take the limit $R \to \infty$, to isolate the universal part of the solution, we have to subtract the divergence of the J-integral by adjusting $v_{\rm tip}$. To leading order $s(l) = 1/\sqrt{l}$, and so (29) yields as $R \to \infty$:

$$v_z^J \approx \frac{\sqrt{\ln R}}{2} + O[(\ln R)^{-1/2}]. \tag{47}$$

Thus in order to cancel the divergence for infinite system size $R \to \infty$, we choose

$$v_{\rm tip} = -\int_0^{\ln R} \frac{1}{4(1+\zeta_2)^{1/2}} d\zeta_2 = -\left.\frac{2(1+\zeta_2)^{1/2}}{2}\right|_0^{\ln R} \approx -\frac{\sqrt{\ln R}}{2},$$

to obtain

$$\begin{aligned}\mathbf{v}(\zeta_1) = &-\int_0^\infty \left[\hat{\kappa}(\zeta_2)\hat{\mathbf{j}}(\zeta_1,\zeta_2) + \frac{\mathbf{e}_z}{4(1+\zeta_2)^{1/2}}\right] d\zeta_2 \\ &- \int_0^\infty \hat{\mathbf{k}}(\zeta_1,\zeta_2)\cdot\mathbf{v}(\zeta_2)\, d\zeta_2 + \int_0^\infty \hat{\mathbf{k}}^s(\zeta_1,\zeta_2)\, d\zeta_2 \cdot \mathbf{v}(\zeta_1).\end{aligned} \tag{48}$$

All integrals are now convergent, so we were able to take the limit $R \to \infty$ in (48). The boundary condition at the tip is that the curvature is $\hat{\kappa}(\zeta = 0) = 1$; the velocity can be shifted so as to ensure $v_z(0) = 0$. Since we understand the asymptotic behavior of the solution of (48) as $\zeta_1 \to \infty$ in detail (we will calculate the next order in the next section), we don't need the solution for large ζ. Instead, we extract the similarity solution from the simulation of an entire bubble, and match it up with the asymptotic behavior.

D. Leading-order matching

We have seen that the inner solution generates a velocity (47) which diverges with $R \to \infty$. This has to match the tip velocity $v_{\rm tip}$ of the outer flow. In units of γ/η, $-v_{\rm tip}$ is the local capillary number ${\rm Ca}_{\rm tip}$ at the tip. In other words, we have ${\rm Ca}_{\rm tip} \approx \sqrt{\ln(R)}/2$. Solving for κ_m, this is equivalent to

$$\kappa_m \propto \ell^{-1} \exp\left(4{\rm Ca}_{\rm tip}^2\right), \tag{49}$$

which agrees with the scaling law proposed earlier by us [15] on the basis of numerical data. There the constant inside the exponential was found to be approximately 3.7, instead of 4 in (49). Our calculation below, incorporating the next order in an expansion in $1/\ln R$, will reveal that this discrepancy comes from the fact that the prefactor in (49) contains a weak dependence on ${\rm Ca}_{\rm tip}$. Note that in [15], the constant was given incorrectly as 1.6, owing to a confusion between natural logarithm and common logarithm.

Coming back to the approximation $\mathbf{v}^{(\rm ext)} \approx v_{\rm tip}\mathbf{e}_z$ in the step from (15) to (16), the external velocity field $\mathbf{v}^{(\rm ext)}$ has z-component $v_z^{(\rm ext)} \approx -{\rm Ca}_{\rm tip}$ with correction of order R^{-1}, while $v_r^{(\rm ext)} \approx -\frac{{\rm Ca}_{\rm tip}}{2R} H(\zeta)$. On the other hand, from the kinematic boundary condition it follows that $v_r \approx -{\rm Ca}_{\rm tip}\frac{dH}{d\zeta}$, which is larger by a factor $R \propto \exp(4{\rm Ca}_{\rm tip}^2)$ than the radial component of the external velocity. Thus the approximation is always valid in the inner region, as anticipated.

III. THE LOCAL APPROXIMATION: NEXT ORDER

To check if the leading-order result (45) is consistent, and to be able to perform the matching to higher order, we now calculate the next order of the inner similarity solution in the limit $l \to \infty$. We will see that individual entries in (19) contain either odd or even powers of $1/\sqrt{l}$, so it is consistent to assume an expansion of the form

$$s = l^{-1/2} + a_1 l^{-3/2} + \cdots, \quad v_z = -l^{1/2}/2 + b_1 l^{-1/2} + \cdots, \quad v_r = -1/2 + c_1 l^{-1} + \cdots, \tag{50}$$

where the coefficients a_1, b_1, c_1 will turn out to be logarithmically dependent on l. Since the leading term in the v_z-equation is $\propto\sqrt{l}$, we now have to calculate terms of order $s \sim 1/\sqrt{l}$, and in the v_r-equation terms of order $s^4 \sim 1/l^2$.

We begin with $v_r^{(J)}$ and $v_z^{(J)}$, as given by (21) and (27), and expand each term. First, the curvature has the form

$$\zeta\hat{\kappa} = \frac{1}{s\sqrt{1+(s+s')^2}} - \frac{s'+s''}{\sqrt{1+(s+s')^2}^3} = \frac{1}{s} - \frac{1}{2s^3} - s' + O(l^{-3/2}), \tag{51}$$

while the kernels are treated by expanding about $l = l_1$:

$$s_2 = s_1 + s_1'\Delta + O(\Delta^2), \quad s_2' = s_1' + s_1''\Delta + O(\Delta^2),$$

and where now s_1' and s_1'' are treated as small parameters. Hence any kernel can be expanded in the form

$$\hat{j}_r(s_1, s_2, s_2', \Delta) \approx \hat{j}_r(s_1, \Delta) + s_1'\left(\Delta\frac{\partial\hat{j}_r}{\partial s_2} + \frac{\partial\hat{j}_r}{\partial s_2'}\right) + s_1''\Delta\frac{\partial\hat{j}_r}{\partial s_2'} + \cdots,$$

where all derivatives are evaluated at $s_2 = s_1$, $s_2' = 0$, and

$$\zeta\hat{\kappa}(l_2) \approx \frac{1}{s_1} - \frac{1}{2s_1^3} - s_1' - \frac{s_1'}{s_1^2}\Delta.$$

As a result, we obtain

$$\begin{aligned} v_r^{(J)} &\approx -\left(\frac{1}{s_1} - \frac{1}{2s_1^3} - s_1'\right)\left[\int_{-\infty}^{\infty}\hat{j}_r(s_1,\Delta)\,d\Delta + s_1'\int_{-\infty}^{\infty}\Delta\frac{\partial\hat{j}_r}{\partial s_2}\,d\Delta\right. \\ &\quad \left. + s_1'\int_{-\infty}^{\infty}\frac{\partial\hat{j}_r}{\partial s_2'}\,d\Delta + s_1''\int_{-\infty}^{\infty}\Delta\frac{\partial\hat{j}_r}{\partial s_2'}\,d\Delta\right] + \frac{s_1'}{s_1^2}\int_{-\infty}^{\infty}\Delta\hat{j}_r\,d\Delta \\ &\equiv -\left(\frac{1}{s_1} - \frac{1}{2s_1^3} - s_1'\right)[I_0 + s_1'I_1 + s_1'I_2 + s_1''I_3] + \frac{s_1'}{s_1^2}I_4, \end{aligned} \tag{52}$$

where we want to calculate this expression to $O(s^4)$ or $O(l^{-2})$. This means we need I_0 to order s^5, I_1 and I_2 to order s^2, I_3 to order s^0, and I_4 to order s^3.

As we have seen, the integrands are characterized by a central peak of characteristic width $\Delta \propto s$, while there is exponential decay in the wings on a scale of unity; cf. (20). To compute the integral from $-\infty$ to ∞, we need a uniform approximation over the whole real line [16], which we find by constructing a composite approximation using van Dyke's matching rule [42,43]. Taking I_0 as an example, we write the inner and outer expansions by expanding in s, holding either $\xi = \Delta/s$ constant (inner expansion) or Δ constant (outer expansion). Thus writing $f(s,\Delta) \equiv \hat{j}_r(s,\Delta)$, the inner expansion is

$$f(s,\Delta) \approx H_Q f \equiv \sum_{n=0}^{Q} f_n(\xi)s^n, \tag{53}$$

where H_Q projects f upon its power expansion up to order Q. We can take Q as an even number, since all $f_{2i-1}(\xi)$ are odd functions [while the $f_{2i}(\xi)$ are even], and do not contribute to the integral. For large ξ, the functions f_n either grow or decay like a power law.

On the other hand, the outer expansions are different for $\Delta > 0$ or $\Delta < 0$:

$$f(s,\Delta) \approx E_{Q+1} f^{\pm} \equiv \sum_{n=0}^{Q+1} F_n^{\pm}(\Delta) s^n, \tag{54}$$

where E_{Q+1} is the corresponding projection of the outer expansion. It is sufficient to expand up to $Q+1$ for the contribution of the inner and outer expansions to the integral to be of the same order. One can verify in each case that $E_{Q+1}H_Q f = H_Q E_{Q+1} f$, which according to the matching rule implies that

$$f(s,\Delta) \approx E_{Q+1} f + H_Q f - H_Q E_{Q+1} f \tag{55}$$

is a uniform approximation to the integrand to the desired order.

To perform the integral, we split the overlap, which has the form

$$H_Q E_{Q+1} f = \sum_{n=-n_-}^{n_+} P_n^{\pm} \Delta^n \equiv P_+^{\pm} + R^{\pm} + P_-^{\pm} \tag{56}$$

into non-negative powers of Δ (i.e., $P_+^{\pm}$), the power $n=-1$ (i.e., $R^{\pm}$), and powers $n<-1$ ($P_-^{\pm}$); again, the upper index denotes the expansion for $\Delta > 0$ (+), the lower index the expansion for $\Delta < 0$ (−). Since the integral over P_+ converges near the origin, while the integral over P_- converges at infinity (we for the moment disregard R, which leads to a divergence both at the origin and at infinity) we regroup as follows to compute the integral:

$$\begin{aligned} I_0 = \int_{-\infty}^{\infty} f(s,\Delta) d\Delta &\approx \int_{-\infty}^{0} (E_{Q+1} f^- - P_-^-) d\Delta \\ &+ \int_0^{\infty} (E_{Q+1} f^+ - P_-^+) d\Delta + 2s \int_0^{\infty} (H_Q f - P_+^+) d\xi, \end{aligned} \tag{57}$$

where now all integrals are convergent. An explicit calculation shows that I_0 vanishes at each order in s, which we checked up to $O(s^7)$. This agrees with (24), which is demonstrated in Appendix A.

Next, we consider I_1 (i.e. $f = \Delta \frac{\partial j_r}{\partial s_2}$), to which in the inner expansion only odd powers of s contribute, and thus $Q = 1, 3, 5, \ldots$. Now $f_1(\xi)$ decays like $1/\xi$ at infinity, indicating a logarithmic behavior after integration. Indeed, the overlap in (56) now contains $R^{\pm} = \pm(s/4 - 3s^3/8)/\xi + O(s^6)$, which is divergent both at the origin and at infinity. To deal with this divergence, we introduce an arbitrary parameter $B > 0$ to split the integrals into two:

$$\begin{aligned} I_1 = \int_{-\infty}^{\infty} f(s,\Delta) d\Delta \equiv I_{\text{out}} + I_{\text{in}} &\approx \int_{-\infty}^{-B} (E_{Q+1} f^- - P_-^-) d\Delta + \int_{-B}^{0} (E_{Q+1} f^- - P_-^- - R^-) d\Delta \\ &+ \int_0^{B} (E_{Q+1} f^+ - P_-^+ - R^+) d\Delta + \int_B^{\infty} (E_{Q+1} f^+ - P_-^+) d\Delta \\ &+ 2s \int_0^{B/s} (H_Q f - P_+^+) d\xi + 2s \int_{B/s}^{\infty} (H_Q f - P_+^+ - R^+) d\xi. \end{aligned} \tag{58}$$

The result cannot depend on the choice of B, and indeed an explicit calculation shows that B drops out.

To make the logarithmic dependence explicit, we rewrite the contribution to I_1 coming from the inner expansion as

$$I_{\rm in} = 2s\int_0^\infty [H_Q f - P_+^+ - R^+(\xi+1)]d\xi + 2s\int_0^{B/s} R^+(\xi+1)\,d\xi$$
$$+2s\int_0^{B/s}[R^+(\xi+1) - R^+(\xi)]d\xi. \tag{59}$$

Now since the argument of $R^+(\xi)$ has been shifted by 1, the first integral of (59) converges at both the lower and the upper limit. Since R^+ is of the form $R^+ = a/\Delta$ (in this case $a = s/4 - 3s^3/8$) the second and third integrals yield

$$\int_0^{B/s}\frac{a}{\xi+1}d\xi + \int_0^{B/s}\left(\frac{a}{\xi} - \frac{a}{\xi+1}\right)d\xi = a\ln B - a\ln s.$$

Thus at order s^2, the logarithmic contribution to I_1 is $-s^2\ln s/2$, while the term $a\ln B$ cancels against a counter-term coming from the outer expansion. Performing the calculations explicitly, we obtain to leading order for the integrals defined in (52)

$$I_1 = s^2\left(\frac{1}{2} + 2j_r^{(1)}\right) - \frac{s^2}{2}\ln s, \quad I_2 = -\frac{s^2}{4}, \quad I_4 = \left(\frac{1}{4} + 2j_r^c - \frac{\ln s}{4}\right)s^3, \tag{60}$$

where

$$j_r^{(1)} = \int_0^\infty\left[\xi\, j_0^{(1)}(\xi) - \frac{1}{4(1+\xi)}\right]d\xi, \quad j_r^c = \int_0^\infty\left[\xi\, j_1(\xi) - \frac{1}{8(1+\xi)}\right]d\xi. \tag{61}$$

Here $j_0^{(1)}(\xi)$ is the constant coefficient in the inner expansion of $\frac{\partial\hat{j}_r}{\partial s_2}$, and $j_1(\xi)$ the linear coefficient in the inner expansion of $\hat{j}_r$. The integral I_3 is of order s^2 and need not be considered. Thus we finally find

$$v_r^{(J)} = -\frac{s'}{s}(I_1 + I_2) + \frac{s'}{s^2}I_4 = s's\left[2j_r^c - 2j_r^{(1)} + \frac{\ln s}{4}\right] + O(s^6). \tag{62}$$

Next we calculate $v_z^{(J)}$, using (27) and (28), calculating terms of $O(s)$. Proceeding by the method of composite approximations described above, we find

$$\int_{-\infty}^\infty\left[\hat{j}_z - H(\Delta)\hat{j}_z^e\right](s_1,\Delta)d\Delta = s^2\left(-\frac{\ln 2}{2} + \frac{\ln s}{2}\right),$$

since

$$\int_0^\infty\left[j_1^{(z)} + \frac{1}{4(1+\xi)}\right]d\xi = -\frac{\ln 2}{4}, \tag{63}$$

where $j_1^{(z)}(z)(\xi)$ is the linear term of the inner expansion of $\hat{j}_z$ (see Appendix A). Taken together, this yields

$$v_z^{(J)} \approx \int_{\ln(2R)}^{l_1}\zeta_2\hat{\kappa}\,\hat{j}_z^e\,dl_2 - s\left(-\frac{\ln 2}{2} + \frac{\ln s}{2}\right). \tag{64}$$

In fact, using (63), the constant $j_r^c - j_r^{(1)}$ in (62) is $j_r^c - j_r^{(1)} = 3/32 - \ln 2/8$, a consequence of the identity

$$\int_0^\infty\left[4\xi\, j_1(\xi) - 4\xi\, j_0^{(1)}(\xi) - 2j_1^{(z)}(\xi)\right]d\xi = \frac{3}{8}, \tag{65}$$

which can be found using the methods of Appendix A.

Now we come to the K-integrals, and begin with the z-equation, for which we need results to $O(s)$. We begin with K_1, defined in (33). Calculating the leading contribution to the first, local integral, and using that $v_z(l_2) - v_z(l_1) = v_z'\Delta + O(\Delta^2)$, we obtain

$$\int_{-\infty}^{\infty} \left[\zeta_2\hat{k}_1 - H(\Delta)\zeta_2\hat{k}_1^e\right][v_z(l_2) - v_z(l_1)]\, dl_2 \approx v_z' \int_{-\infty}^{\infty} \left[\zeta_2\hat{k}_1 - H(\Delta)\zeta_2\hat{k}_1^e\right]\Delta d\Delta.$$

The integral is of order s^2, and $v_z' \sim s$, and hence the local integral need not be considered at this order. We are left with

$$K_1 \approx \int_{l_1}^{\ln(2R)} \zeta_2\hat{k}_1^e v_z(l_2)\, dl_2 - v_z(l_1) \int_{l_1}^{\ln(2R)} \zeta_2\hat{k}_1^e\, dl_2. \tag{66}$$

Using (50), one finds that to leading order $\zeta_2\hat{k}_1^e \approx -3ss'/2 = 3(4l_1^2) + O(l_1^{-3})$ and $\zeta_2\hat{k}_1^e v_z = -3/(8l_1^{3/2}) + O(l_1^{-5/2})$, so that up to an R-dependent constant $C(R)$

$$K_1 \approx -\frac{3}{4\sqrt{l_1}} - v_z(l_1)\frac{3}{4l_1} + C(R) = -\frac{3}{8\sqrt{l_1}} + C(R). \tag{67}$$

The constant $C(R)$ will be calculated later, once we have a description of the profile over the entire drop.

As for K_3, defined in (35), $\hat{k}_3^e \approx -3s^2s'/2 \approx 3/(4l^{5/2})$ at leading order, and since $v_r \approx -1/2$, the second, nonlocal integral makes a contribution $\propto 1/l_1^{3/2}$, which is subdominant in the z-equation. Thus as was shown in Sec. II C, according to (42) we have $K_3 \approx v_r s/2$.

Coming to the r-equation, we have to calculate to order $O(s^4)$. Using that $v_z(l_2) - v_z(l_1) = \Delta v_z' + \cdots$, it is sufficient to calculate the leading contribution

$$\int_{-\infty}^{\infty} \Delta\zeta_2\hat{k}_2(s, \Delta)\, d\Delta = -\frac{s}{2} + \frac{3s^3}{4} + O(s^5),$$

and thus we obtain

$$K_2 = v_z'\left[-\frac{s}{2} + \frac{3s^3}{4}\right] + O(s^5). \tag{68}$$

Finally we compute K_4 to the next order, using (36). We can approximate $\hat{k}_4^{s,e} = -3s^3s'/(4(1 + s^2)^{5/2} \approx -3(s^4)'/16$, and thus the nonlocal integral becomes

$$\int_{l_1}^{\ln(2R)} \hat{k}_4^{s,e}\, dl_2 \approx -\frac{3}{16}s^4\Big|_{l_1}^{\infty} \approx \frac{3s_1^4}{16}.$$

The local part can be approximated as

$$\begin{aligned}
&\int_{-\infty}^{\infty} \zeta_2\left\{\hat{k}_4 v_r(l_2) - \left[\hat{k}_4^s - H(\Delta)\hat{k}_4^{s,e}\right]v_r(l_1)\right\} dl_2 \approx v_r(l_1)\int_{-\infty}^{\infty} \zeta_2\left[\hat{k}_4 - \hat{k}_4^s + H(\Delta\hat{k}_4^{s,e})\right] dl_2 \\
&+ v_r'(l_1)\int_{-\infty}^{\infty} \zeta_2\hat{k}_4\Delta\, dl_2 \approx v_r(l_1)\left[\int_{-\infty}^{\infty} \zeta_2\left(\hat{k}_4 - \hat{k}_4^s + H(\Delta)\hat{k}_4^{s,e}\right)(s_1, \Delta)\, d\Delta\right. \\
&\left. + s_1'\int_{-\infty}^{\infty}\left(\Delta\frac{\partial\left\{\zeta_2\left[\hat{k}_4 - \hat{k}_4^s + H(\Delta)\hat{k}_4^{s,e}\right]\right\}}{\partial s_2} + \frac{\partial\left\{\zeta_2\left[\hat{k}_4 - \hat{k}_4^s + H(\Delta)\hat{k}_4^{s,e}\right]\right\}}{\partial s_2'}\right)d\Delta + O(s_1'')\right] \\
&+ v_r'(l_1)\int_{-\infty}^{\infty} \Delta\zeta_2\hat{k}_4(s_1, \Delta)\, d\Delta \equiv v_r(l_1)(I_0 + s_1'I_1) + v_r'(l_1)I_2.
\end{aligned} \tag{69}$$

We find that

$$I_0 = -1 + \frac{s^2}{4} + O(s^4), \quad I_1 = \frac{3s}{8},$$

while $I_2 \sim s^2$, so that $v_r' I_2 \sim l^{-3}$, which does not need to be considered at this order. As a result, we finally obtain from (36)

$$K_4 = v_r\left(-1 + \frac{s^2}{4} + \frac{3s's}{8} - \frac{3s^4}{16}\right). \tag{70}$$

Inserting everything into (19), the equations become to second order (which means including $s \propto l^{-1/2}$ for the z-equation, and $s^4 \propto l^{-2}$ for the r-equation):

$$v_z = v_{\rm tip} + \int_{\ln(2R)}^{l} \zeta_2 \hat{\kappa} \hat{f}_z^e \, dl_2 - s\left(-\frac{\ln 2}{2} + \frac{\ln s}{2}\right) + \frac{3}{8\sqrt{l}} - C(R) - \frac{v_r s}{2}, \tag{71}$$

$$0 = s's\left(\frac{3}{16} - \frac{\ln 2}{4} + \frac{\ln s}{4}\right) - v_z'\left(-\frac{s}{2} + \frac{3s^3}{4}\right) - v_r\left(\frac{s^2}{4} + \frac{3s's}{8} - \frac{3s^4}{16}\right). \tag{72}$$

This has to be solved together with the kinematic condition

$$\frac{dH}{d\zeta} = \frac{v_r}{v_z},$$

which yields

$$\frac{dH}{d\zeta} = s + s' = \frac{v_r}{v_z}. \tag{73}$$

To find the right form of the solution to the system (71)–(73), we eliminate constants of integration by differentiating (71) with respect to l, and eliminate v_r using (73). Putting $s = l^{-1/2} + \delta_1$ and $v_z = -l^{1/2}/2 + \delta_2$, we linearize about the leading-order solution (45). The resulting system of ordinary differential equations for δ_1 and δ_2 can be solved to leading order as $l \to \infty$, from which we derive the structure of the solution as

$$s = (l - l_0)^{-1/2} + (A_1 \ln l + A_2 \ln^2 l)(l - l_0)^{-3/2}, \tag{74}$$

$$v_z = v_0 - \frac{\sqrt{l - l_0}}{2} + (v_1 + B_1 \ln l + B_2 \ln^2 l)(l - l_0)^{-1/2}. \tag{75}$$

The arbitrary shift l_0 is an expression of the fact that Eqs. (71)–(73) are translationally invariant.

Using (74) and (75), we expand as follows:

$$\zeta_2 \hat{\kappa} \hat{f}_z^e = -\frac{1}{4\sqrt{l - l_0}} + \left[\frac{1}{2} - \frac{A_1}{4}\ln l - \frac{A_2}{4}\ln^2 l\right]\frac{1}{\sqrt{l - l_0}^3} + \cdots.$$

Inserting this into the differentiated version of (71), and solving it together with (72) for A_1, A_2, B_1, and B_2, we obtain

$$s = \frac{1}{\sqrt{l - l_0}} + 2\left[\left(\frac{9}{16} - \frac{\ln 2}{4}\right)\ln l - \frac{\ln^2 l}{16}\right](l - l_0)^{-3/2} + \cdots, \tag{76}$$

$$v_z = v_0 - \frac{\sqrt{l - l_0}}{2} + \left[\frac{1}{4} + \left(\frac{9}{16} - \frac{\ln 2}{4}\right)\ln l - \frac{\ln^2 l}{16}\right](l - l_0)^{-1/2} + \cdots, \tag{77}$$

$$v_r = -\frac{1}{2} + \frac{1}{2(l - l_0)} + \cdots, \tag{78}$$

where l_0 has been chosen so that any constant coefficient of $l^{-3/2}$ in the expansion of s is zero. The constant v_0 is a constant of integration; by matching to the outer solution we will see below that v_0 has to vanish: $v_0 = 0$. In Fig. 3 (left) we show $dH d\zeta = s + s'$ fitted to the asymptotic form (76), using l_0 as the only fit parameter. The result is $l_0 = 0.1$ and yields a very good fit. As far as the matching to the outer solution is concerned, the constant l_0 contains all the information about the

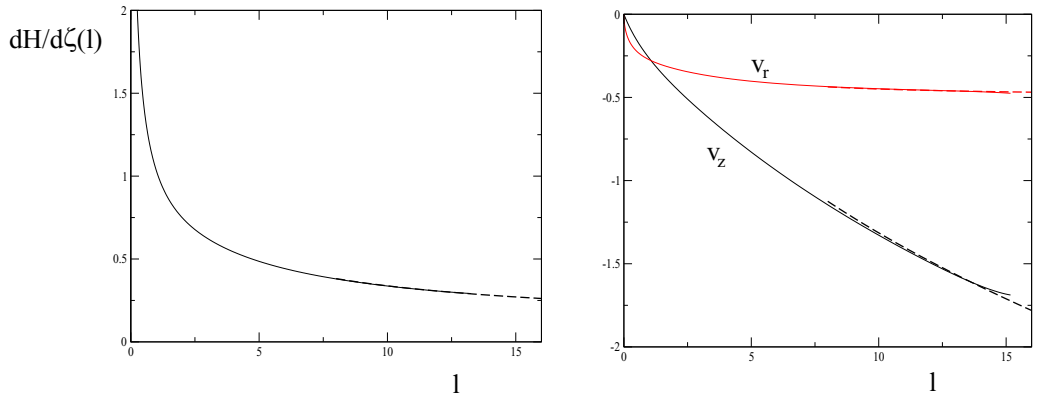

FIG. 3. Left: The slope $dHd/\zeta(l)$, rescaled in similarity form, compared with the asymptotics (76), where $l_0 = 0.1$ was adjusted. Right: The two components of the velocity field v_z (black) and v_r (red), compared with (77) and (78), respectively.

very tip of the similarity solution, where the curvature is unity. Using this constant, the asymptotics of both v_z and v_r can be predicted without adjustable parameters (on the right of Fig. 3), yielding very good agreement, without adjustable parameters.

IV. OUTER, SLENDER BODY SOLUTION

The outer solution is based on the idea that for a strong external flow (large Ca), the drop is slender (its typical radial extension is much smaller than its length). Using slenderness, Taylor [6] suggested to represent the effect of the drop on the external flow as a distribution of two-dimensional point sources along the axis. This idea was worked out systematically in [7] using slender body theory [16]. We now recall the important results of this theory for an inviscid bubble in the hyperbolic flow (3); see Fig. 2.

The outer flow problem is nondimensionalized as follows: as the length scale we choose the drop half-length ℓ, the inverse extension rate G^{-1} [see (3)] as the timescale, and $G\eta$ as the pressure scale. Denoting dimensionless outer variables with an overbar, the external flow is now

$$\overline{v}_z^{(\mathrm{ext})} = \overline{z}, \quad \overline{v}_r^{(\mathrm{ext})} = \overline{r}/2,$$

and the Stokes equation is $\nabla\overline{p} = \triangle\overline{\mathbf{v}}$. Finally, the normal stress boundary condition is

$$\mathbf{n}\cdot\overline{\boldsymbol{\sigma}}\cdot\mathbf{n} = \epsilon\overline{\kappa}, \quad \epsilon \equiv \frac{\gamma}{G\eta\ell}. \tag{79}$$

A strong flow corresponds to small ϵ, which will be our expansion parameter. It can be interpreted as the inverse of the local capillary at the tip, since $-G\ell$ is the unperturbed velocity at the tip: $\epsilon = 1/\mathrm{Ca}_{\mathrm{tip}}$.

Since the flow is axisymmetric, we can introduce the stream function to write

$$\overline{v}_r = -\frac{1}{\overline{r}}\frac{\partial\psi}{\partial\overline{z}}, \quad \overline{v}_z = \frac{1}{\overline{r}}\frac{\partial\psi}{\partial\overline{r}}. \tag{80}$$

The idea, as proposed originally in [6], is to write ψ as the sum of the outer flow's contribution and a small perturbation, coming from a distribution of sources and Stokeslets along the axis:

$$\psi = \frac{\overline{r}^2\overline{z}}{2} + \int_{-1}^{1}\frac{f(\tilde{z})\overline{r}^2}{\sqrt{\overline{r}^2+(\overline{z}-\tilde{z})^2}}\,d\tilde{z} - \int_{-1}^{1}\frac{g(\tilde{z})(\overline{z}-\tilde{z})}{\sqrt{\overline{r}^2+(\overline{z}-\tilde{z})^2}}\,d\tilde{z}, \tag{81}$$

which by definition satisfies Stokes' equation. Apart from the two Eqs. (79), we have to satisfy the kinematic condition

$$\psi|_{\bar{r}=\bar{h}} = 0, \tag{82}$$

which are three equations for the three unknowns $\bar{h}$, f, and g, which are to be solved at each order.

Buckmaster's [7] calculation shows that the solution has the structure

$$\bar{h} = \epsilon h_0 + \epsilon^3 h_1 + \cdots, \quad f = \epsilon^2 f_0 + \epsilon^4 f_1 + \cdots, \quad g = \epsilon^2 g_0 + \epsilon^4 g_1 + \cdots. \tag{83}$$

At each order, (82) and the normal stress balance (79) are a closed set of equations for $\bar{h}$ and g; f can then be calculated from the tangential stress balance. At lowest order, the result is [7]

$$h_0 = \frac{1}{4}(1-\bar{z}^2), \quad f_0 = -\frac{\bar{z}}{16}(1-\bar{z}^2), \quad g_0 = \frac{1-\bar{z}^2}{64}(1-5\bar{z}^2), \tag{84}$$

which corresponds to the solution found in [6]. We consider only the generic and stable solution [9], for which h_0 has a quadratic maximum at $\bar{z} = 0$.

At the next order, one finds

$$h_1(\bar{z}) = \bar{z}^2 \int_{-1}^{\bar{z}} \frac{Q(s)}{s^2}\, ds, \tag{85}$$

where $Q(s)$ is of the form

$$Q(s) = -2\frac{H_1(\bar{z}) + p_{\inf} h_0^2(\bar{z})}{\bar{z}(1-\bar{z}^2)},$$

and $H_1(\bar{z})$ is a function given in terms of integrals over the first-order solution [7], which are easily calculated. In an expansion around $s = 0$ (the center of the drop), Q has the structure $Q = Q_{-1}s^{-1} + Q_1 s + O(s^3)$. The most singular term $Q_{-1}s^{-1}$, after integration, cancels against the factor $\bar{z}^2$ in front of the integral and contributes to the constant $h_1(0)$.

The term $Q_1 s$ yields a logarithm after integration, and would result in the profile no longer being analytic. Thus the constant of integration $p_{\inf}$ that appears in the pressure at second order must be chosen such that $Q_1 = 0$, resulting in $p_{\inf} = 6 - 12\ln 2 + 4\ln\epsilon$. With this choice, the result for (85) is

$$\begin{aligned} h_1(\bar{z}) = {} & \frac{\bar{z}^2 \mathrm{Li}_2(\bar{z}^2)}{8} + \frac{27\bar{z}^4 - 24\bar{z}^2 - 3}{192}\ln(1-\bar{z}^2) + \frac{27\bar{z}^4 - 48\bar{z}^2 + 21}{96}\ln(\epsilon) \\ & + \frac{-162\bar{z}^4 + 288\bar{z}^2 - 126}{192}\ln(2) + \frac{23}{64}(1+\bar{z}^4) - \frac{4\pi^2 + 138}{192}\bar{z}^2, \end{aligned} \tag{86}$$

where

$$\mathrm{Li}_2(x) \equiv -\int_0^z \frac{\ln(1-u)}{u}\, du$$

is the dilogarithm.

Near the ends, $h_1 \approx (1-|\bar{z}|)\ln(1-|\bar{z}|)$, which becomes large compared to the conical solution at leading order, which means that the perturbation expansion breaks down near the ends. This is expected, since the slenderness assumption is violated at the tips. Instead, we have to use the similarity solution of the previous section, and match it to the perturbative result. At the center of the drop,

$$h_1(0) = \frac{7}{32}\ln\epsilon - \frac{21}{32}\ln 2 + \frac{23}{64}, \tag{87}$$

which agrees with [9]. Otherwise $h_1(z)$ has a regular expansion in z^2 at $z = 0$, as anticipated.

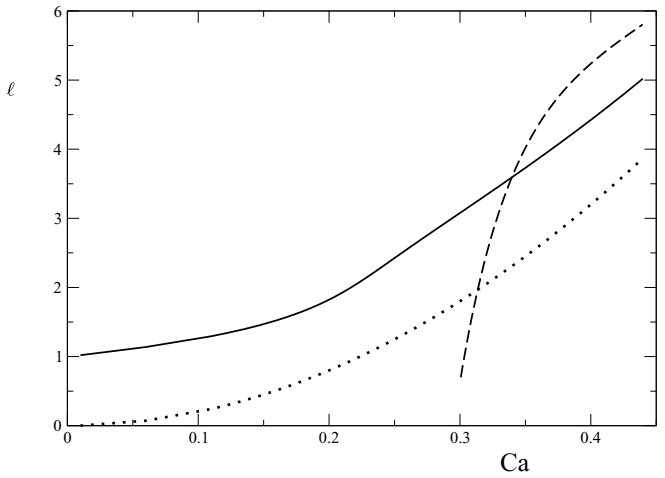

FIG. 4. The drop half-length ℓ as function of the capillary number $\mathrm{Ca} = GR_d\eta/\gamma$ for for a bubble in the flow (3); see Fig. 2. The solid line is the result of our boundary integral simulation [15], the dotted line is the leading-order result [6], the dashed line is (89).

To determine ℓ, we compute the volume of the drop:

$$V = 2\pi\ell^3 \int_0^1 \overline{h}^2(\overline{z})\, d\overline{z}.$$

Now $\epsilon = a/\ell$, where $a = \gamma/(G\eta)$ is a characteristic length of the outer flow. To leading order, $\overline{h} = \epsilon h_0$, and

$$\int_0^1 h_0^2\, d\overline{z} = \frac{1}{30},$$

so that $V = \pi a^2\ell/15$. Thus since $\mathrm{Ca} = R_d/a$, one finds $\ell = 20\mathrm{Ca}^2 R_d$ to leading order [6].

Expanding to next order in ϵ^2, we have

$$V = 2\pi\ell^3\left[\epsilon^2\int_0^1 h_0^2\, d\overline{z} + 2\epsilon^4\int_0^1 h_0 h_1\, d\overline{z}\right] = 2\pi\ell^3\left[\frac{\epsilon^2}{30} + \epsilon^4\left(\frac{50\,863}{661\,500} + \frac{\ln\epsilon}{21} - \frac{227\ln 2}{1575}\right)\right]. \tag{88}$$

Inserting the first-order result $\epsilon = 1/(20\mathrm{Ca}^3)$ into the second-order term, this can be solved to give

$$\frac{\ell}{R_d} = 20\mathrm{Ca}^2 - \frac{3}{2\mathrm{Ca}^4}\left[\frac{50\,863}{661\,500} - \frac{\ln(20\mathrm{Ca}^3)}{21} - \frac{227\ln 2}{1575}\right]. \tag{89}$$

This result is compared to a full numerical simulation in Fig. 4. We will see below that the prediction of (89) will not be changed by the explicit inclusion of the inner solution, although the solution itself breaks down at the ends.

For the capillary numbers that can be realized while still resolving the entire solution, the agreement is mediocre: while the leading order result significantly underpredicts the drop length, including the next order leads to an overprediction. For example in the case of Fig. 2, for which $\mathrm{Ca} = 0.4393$, and drop radius $R_d = 1$, (89) yields $\ell = 3.86$ at first order, and $\ell = 5.79$ at the next order, while numerically we find $\ell = 4.797$, a 20% overprediction at second order. Solving the nonlinear Eq. (88) for ℓ directly yields $\ell = 5.65$. However, this does not mean slender body theory is deficient, since Ca is quite small in our example. Since the aspect ratio of the drop is $1/(80\mathrm{Ca}^3)$ to first order, slenderness is well verified even for $\mathrm{Ca} \sim 1$. Indeed, for $\mathrm{Ca} = 1$ first- and second-order

predictions for ℓ differ only by 1%. More importantly, we will see below that slender body theory is a crucial ingredient of the composite solution for the crossover between the tip and the bulk of the drop, which works extremely well, even for $\mathrm{Ca} \lesssim 1/2$.

In order to match the outer solution to the tip region, we investigate the limit $\bar{z} \to -1$ of the slender-body solution, going toward the tip, and introduce $\xi = (z+\ell)/\ell = 1+\bar{z}$:

$$h_1(\xi) = \tfrac{1}{16}(-2\ln\epsilon - \ln\xi + 5\ln 2 - 4)\xi + O(\xi^2). \tag{90}$$

In other words, the inner limit of the outer expansion becomes

$$\bar{h}_{\mathrm{in}} = \frac{\epsilon\xi}{2} + \frac{\epsilon^3\xi}{16}[-\ln(\epsilon^2\xi) + 5\ln 2 - 4] + \cdots, \tag{91}$$

where the term $\ln\xi$ signals the breakdown of the outer expansion, as observed in [7]. Using (80) and expanding the integrals (81) in ϵ, the velocity field can also be calculated to second order, with the results

$$\bar{v}_z = \bar{z} + \frac{\epsilon^2\bar{z}}{16}(3\bar{z}^2 - 1)[3 - 6\ln 2 + 2\ln\epsilon + \ln(1-\bar{z}^2)] + O(\epsilon^4) \tag{92}$$

and

$$\begin{aligned}\bar{v}_r = &-\frac{\epsilon\bar{z}^2}{2} - \frac{\epsilon^3\bar{z}^2}{96}\{\pi^2 - 138\bar{z}^2 - 24\mathrm{Li}_2(\bar{z}^2) + 45(1-\bar{z}^2)\ln[\epsilon^2(1-\bar{z}^2)] \\ &- 270(1-\bar{z}^2)\ln 2 + 126\} + O(\epsilon^5).\end{aligned} \tag{93}$$

Expanding this for small $\xi = 1+\bar{z}$, we obtain

$$\bar{v}_z = -1 + \frac{\epsilon^2}{8}[-\ln(\epsilon^2\xi) + 5\ln 2 - 3] + O(\xi, \epsilon^4), \quad \bar{v}_r = -\frac{\epsilon}{2} + \frac{\epsilon^3}{8} + O(\xi, \epsilon^5). \tag{94}$$

V. MATCHING TO THE DROP

Now we match the inner similarity solution $H(\zeta)$ to the outer solution $\bar{h}(\bar{z})$. Outer and inner variables are connected by

$$\zeta = \xi R, \quad H = R\bar{h}, \quad \mathbf{v} = \epsilon^{-1}\bar{\mathbf{v}}, \tag{95}$$

where we recall that $\zeta = (z+\ell)\kappa_m$ and $R = \ell\kappa_m$.

The expansion (76)–(78) represents the outer limit of the inner solution near the tip for $\zeta \to \infty$, while (91)–(94) is the inner limit $\xi \to 0$ of the outer solution. We will now compare the two and construct a composite solution, valid everywhere.

To compare inner and outer expansions, we write the outer limit of the inner expansion [cf. (76)]:

$$\begin{aligned}\bar{h} &= R^{-1}H(\xi R) = \xi s(\xi R) \\ &= \frac{\xi}{\sqrt{\ln(R\xi)}} + 2\xi\left\{\frac{l_0}{4} + \left(\frac{9}{16} - \frac{\ln 2}{4}\right)\ln(\ln(R\xi)) - \frac{\ln^2[\ln(R\xi)]}{16}\right\}[\ln(R\xi)]^{-3/2} + \cdots,\end{aligned}$$

which in the limit of $R \gg \xi$ can be written as

$$\bar{h} = \frac{\xi}{\sqrt{\ln R}} + \xi\left[-\frac{\ln\xi}{2} + \frac{l_0}{2} + \left(\frac{9}{8} - \frac{\ln 2}{2}\right)\ln(\ln R) - \frac{\ln^2(\ln R)}{8}\right](\ln R)^{-3/2} + \cdots. \tag{96}$$

Comparing (96) to (91), we identify $\epsilon = 2/\sqrt{\ln R}$ at leading order. Since $\epsilon = \mathrm{Ca}_{\mathrm{tip}}^{-1}$, this corresponds exactly to our previous matching result (49). To ensure matching at the next order, we put

$$\epsilon = \frac{2}{\sqrt{\ln R}} + \left[l_0 - 3\ln 2 + 4 + \left(\frac{5}{4} - \ln 2\right)\ln(\ln R) - \frac{\ln^2(\ln R)}{4}\right](\ln R)^{-3/2} + \cdots, \tag{97}$$

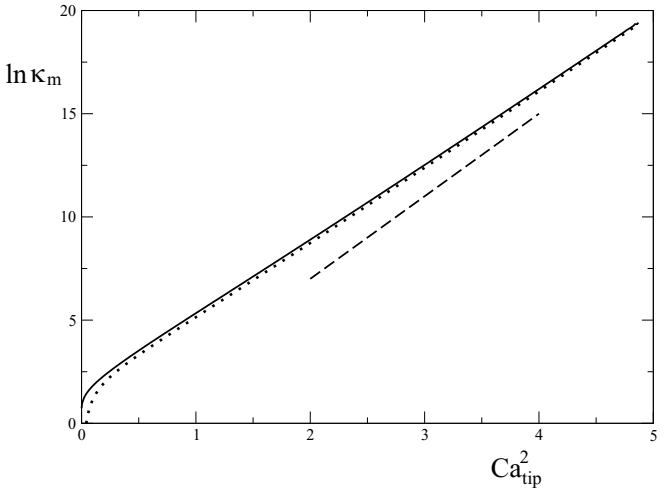

FIG. 5. The natural logarithm of the tip curvature as a function of the square of the local capillary number $\mathrm{Ca}_{\mathrm{tip}}$ (solid line) for a bubble in the hyperbolic flow (3), as shown for a particular capillary number in Fig. 2. The dotted line is the theoretical prediction (98). For comparison, the dashed line has a constant slope of 4, corresponding to the leading-order result (49).

in which case (96) and (91) become identical, when expanded consistently. It is straightforward to confirm that with the same choice of (97), the radial component of the velocity field (78) in the outer limit of the inner expansion becomes identical to $\overline{v}_r$ of (94). If in addition the constant v_0 in (77) is chosen to vanish, (77) also becomes identical to $\overline{v}_z$ of (94), which completes the matching. Writing (97) in terms of the local capillary number $\mathrm{Ca}_{\mathrm{tip}}$, we find an improved estimate for the tip curvature:

$$\kappa_m \approx \frac{C}{\ell} e^{4\mathrm{Ca}_{\mathrm{tip}}^2}, \tag{98}$$

where the prefactor

$$C = \exp\left[l_0 - 3\ln 2 + 4 + 2\left(\tfrac{5}{4} - \ln 2\right)\ln(2\mathrm{Ca}_{\mathrm{tip}}) - \ln^2(2\mathrm{Ca}_{\mathrm{tip}})\right]$$

depends itself slowly on $\mathrm{Ca}_{\mathrm{tip}}$. In Fig. 5 the tip curvature κ_m, taken from a numerical simulation of an inviscid bubble in a hyperbolic flow [15], is compared to the second-order result (98). The agreement is very good, without any adjustable parameters. For comparison, we show a line of constant slope 4, which would be the result of leading-order matching (49). Since in reality the prefactor C is weakly dependent on $\mathrm{Ca}_{\mathrm{tip}}$, the local slope is slightly smaller than that; in [15] it was estimated as 3.7. In addition, the second-order solution fixes the prefactor measured relative to the drop size ℓ, which was undetermined at leading order.

To construct a composite solution, valid everywhere inside the drop, we note that inner and outer solutions have the identical form (76) and (91). As usual [43], a composite solution is obtained by adding inner and outer solutions together, and subtracting the solution valid in the overlap region:

$$h = \ell\overline{h}\left(\frac{z}{\ell}\right) + \kappa_m^{-1} H[(z+\ell)\kappa_m] - \ell\overline{h}_{\mathrm{in}}. \tag{99}$$

The composite solution (99) (dotted line) is compared to a full numerical solution of a bubble (solid line) in Fig. 6. To be able to see the details of the crossover from the tip region to the bulk of the drop, we plot the interface slope as a function of the logarithm of the distance from the tip, over a wide range of scales. The agreement is almost perfect, except in the interior of the bubble,

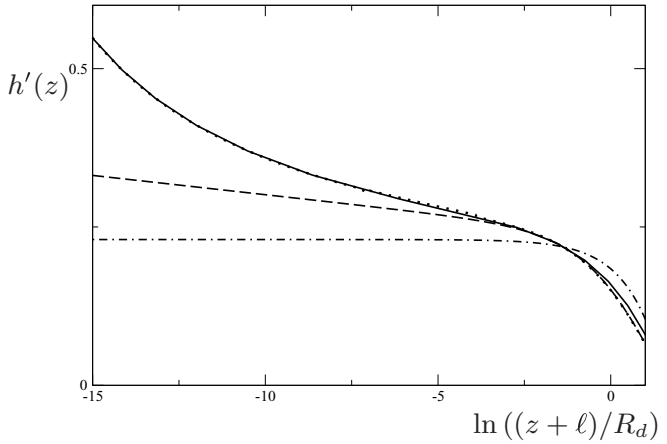

FIG. 6. The interface slope $h'(z)$ of an inviscid drop (or bubble) in the flow (3) at $\mathrm{Ca} = 0.4369$, $R_d = 1$ (solid line), as function of the logarithmic distance from the tip $\ln((z+\ell)/R_d)$. The slope of the composite solution (99) is the dotted line, with the numerical values $\ell = 4.976$ and $\kappa_m = 1.611 \times 10^8$ as input parameters. The slope of the outer solution (83) is shown as the dashed line, and the result of the leading-order solution [6] is shown as the dot-dashed line.

owing to the slow convergence of the outer solution, as manifested in Fig. 4. For comparison, we also plot the result of the outer solution. The dot-dashed line is the leading-order slender body theory [6], which asymptotes to a conical shape near the tip, with constant slope. Including the next order (dashed line) means one captures a first glimpse of the true behavior of the slope, with the slope increasingly linearly with the logarithm of the distance from the tip, while the true solution varies like the square root of the logarithmic distance. Owing to this extremely slow variation, corrections to the leading-order solution are not confined to an exponentially small region, as claimed in [7], but are spread out over all length scales, from the tip size to the length of the drop.

In obtaining (98), we have used the matching condition (97) together with the identification $\epsilon = \mathrm{Ca}_{\mathrm{tip}}^{-1}$. An alternative way to obtain the same answer is to realize that $v_{\mathrm{tip}} = -\mathrm{Ca}_{\mathrm{tip}}$, since by definition v_{tip} is the tip velocity in units of γ/η. Thus we can calculate v_{tip} directly by inserting (77) into (71), which yields

$$-\frac{\sqrt{l}}{2} + \left[\frac{l_0}{4} + \frac{1}{4} + \left(\frac{9}{16} - \frac{\ln 2}{4}\right)\ln l - \frac{\ln^2 l}{16}\right]\frac{1}{\sqrt{l}} = v_{\mathrm{tip}} + \int_{\ln(2R)}^{l} \zeta_2 \overline{\kappa}\, \hat{j}_z^e dl_2 + \left[\frac{5}{8} + \frac{\ln 2}{2} + \frac{\ln l}{4}\right]\frac{1}{\sqrt{l}} - C(R). \tag{100}$$

However, now we have to evaluate the integral in (100), as well the integral underlying $C(R)$, cf. (67). Since the integration is over the entire drop, we need a uniformly valid expression for the integrands. The details are somewhat involved, so they have been moved to Appendix B. The result is that, up to orders of $1/\sqrt{\ln R}$,

$$\int_{\ln(2R)}^{l} \zeta_2 \overline{\kappa}\, \hat{j}_z^e dl_2 = -\frac{\sqrt{l}}{2} + \left[\frac{l_0}{4} - \frac{3}{8} - \frac{\ln 2}{2} + \left(\frac{5}{16} - \frac{\ln 2}{4}\right)\ln l - \frac{\ln^2 l}{16}\right]\frac{1}{\sqrt{l}} + \frac{\sqrt{\ln 2R}}{2} - \left[\frac{l_0}{4} - \frac{3}{8} - \frac{\ln 2}{2} + \left(\frac{5}{16} - \frac{\ln 2}{4}\right)\ln(\ln 2R) - \frac{\ln^2(\ln 2R)}{16}\right]\frac{1}{\sqrt{\ln 2R}} - \frac{3}{4\sqrt{\ln R}} \tag{101}$$

and

$$C(R) = \frac{5}{8\sqrt{\ln R}}. \tag{102}$$

Inserting (101) and (102) into (100), the l-dependence cancels, and we are left with

$$v_{\rm tip} = -\frac{\sqrt{\ln R}}{2} + \left[\frac{l_0}{4} + 1 - \frac{3\ln 2}{4} + \left(\frac{5}{16} - \frac{\ln 2}{4}\right)\ln(\ln R) - \frac{\ln^2(\ln R)}{16}\right]\frac{1}{\sqrt{\ln R}}.$$

Using $\epsilon = -1/v_{\rm tip}$, this is easily seen to be exactly the same as (97), a remarkable check of the consistency of the matching procedure!

VI. DISCUSSION

In this paper, we investigated the tip region of bubbles in strong flows, showing the tip size remains finite. Thus surface tension is always strong enough to keep the surface regular in a steady, axisymmetric flow, as long as the capillary number remains finite. However, as the flow strength increases, a singular tip is approached very rapidly. The flow considered here has some similarities with the two-dimensional, converging flows which create free-surface cusps [31,33]. However, in the two-dimensional, viscous flow case the cusp tip is regularized on a scale which decreases exponentially with the capillary number, whereas in our three-dimensional, axisymmetric case the size decreases much more quickly, exponentially with the *square* of the capillary number. This is in line with the intuition that for tips the focusing is much stronger, since streamlines converge radially onto a single point, while for cusps in three dimensions the forcing is along a line. Thus our solution represents a worst-case scenario, and a stationary free surface with surface tension always remains smooth, at least in the mathematical sense, based on a continuum description down to arbitrarily small scales.

The mechanism for the exponential tip size dependence of the two-dimensional cusp is also very different from what is observed in three dimensions [31]. The tip of the cusp represents a forcing of the fluid by a force of strength 2γ, which would lead to a logarithmic singularity if it were a true point force. This singularity is cut off on the scale of the tip, which leads to a tip size which is exponentially small in the capillary number. However, in three dimensions the tip represents a forcing which is vanishingly small in the limit of small tip size, and hence the same argument does not work here. As we have seen, a nonlocal argument has to be used instead. The shape of the interface is also different, in that in two dimensions the width of the cusp scales like the distance from the tip to the power $3/2$, while in three dimensions both length scales are of the same order, but with logarithmic corrections.

The similarity solution for the drop ends is another example of slow convergence [39], observed, for example, for mean curvature flow [44–46], or for the pinch-off of a bubble in an ideal fluid [47]. In fact, the leading-order nonlinear equation for $s(l)$ is the same as that for the scaling exponent $\delta(\tau)$, which in cavity collapse describes the approach to the fixed point [39], p. 224. In the time-dependent problem, the role of l is taken by the logarithm τ of the time distance to the pinch-off singularity. Slow convergence is associated with vanishing eigenvalues around the fixed point [39], leading to a variation of exponents on a logarithmic scale.

Our calculation of the tip curvature, both theoretically and numerically, demonstrates that the tip size is extremely small, even at moderate values of the capillary number. For a capillary number of slightly less than $1/2$ (see the example of Fig. 2), and for a bubble of radius 1 mm, the tip size would formally be in the order of 10^{-10} m. This size can be reached in our simulations, based on continuum theory, but becomes meaningless as far as an actual experiment is concerned, the tip being smaller than the size of an atom.

To further illustrate the remarkably rapid shrinking of the tip size with flow strength, we estimated the extrapolated tip size, based on continuum theory, for the experimental picture in Fig. 1 (left), for which $\mathrm{Ca} = 0.7$; in that case, the tip size would already be 10^{-89} m! The reason

for this steep rise is that according to (89), the drop length increases with capillary number, which moves the tip to a place where the flow is stronger. Thus, as already noted in [15], the tip curvature increases like the exponential of Ca^6, and quickly reaches sizes at which continuum theory breaks down.

However, the smallness of the tip curvature in many practical situations does not imply that one can ignore the singular behavior near the tip and replace the end by a conical solution solution as predicted in the leading-order slender body analysis. Instead, as shown in Fig. 6, the logarithmic variation of the slope extends over all scales, up to the scale of the drop.

Apart from issues with the applicability of continuum theory, a fully resolved simulation at capillary numbers higher than $1/2$, for which the tip size might be close to a hundred orders of magnitude smaller than the drop, as we have seen above, is hardly feasible. However, simply under-resolving the simulation could lead to numerical instability and results of uncertain accuracy. Instead, we believe our solution can be used to implement effective boundary conditions on a scale much larger than the true tip size, since the asymptotic behavior of the interface slope is now known. This boundary condition will depend on the resolution of the numerics, since the slope is a scale-dependent quantity.

Finally, there are many opportunities to extend our calculation to related problems. One of the most interesting problems would be to include an inner fluid, which will lead the solution to break down at a finite capillary number. Instead, it is often observed that a tiny jet is ejected from the tip, the so-called tipstreaming phenomenon [3,21]. The jet size can be in the order of microns [22,48–50], but it is not known which parameters set the smallest possible jet size. We hope our calculation opens the door to address this question systematically, working directly on the basis of the Stokes equation.

APPENDIX A: INTEGRALS OVER CONES

To demonstrate (24), we consider the conical surface $H = s\zeta$ for $0 \leqslant \zeta \leqslant R$, where at $\zeta = R$ the cone is closed in smooth, axisymmetric fashion. On the mantle of the cylinder, $\kappa = 1/(\zeta_2 s\sqrt{1+s^2})$. Assuming for simplicity that the viscosity inside and outside of the cylinder is η, the boundary integral equation is

$$\mathbf{v}(\mathbf{x}_1) = -\int_S \kappa \mathbf{J}\cdot\mathbf{n}\, d\sigma_2.$$

For reasons of symmetry, the cone can move only along the axis, and so $v_r = 0$. As a result, and transforming to $l_2 = \ln\zeta_2$ as in (17), we find

$$0 = -\frac{1}{s\sqrt{1+s^2}}\int_{-\infty}^{\infty} \hat{j}_r(l_1, l_2)\, dl_2,$$

where we have taken the limit $R \to \infty$. Using that for a cone, $\hat{j}_r(l_1, l_2) = \hat{j}_r(s, \Delta)$, and passing to Δ as the integration variable, we obtain (24).

More identities can be derived from (6). Transforming to logarithmic variables, and using the same cone as above for the surface, one obtains

$$\int_{-\infty}^{\infty} \zeta_2 \hat{k}_1^s(s, \Delta)\, d\Delta = \frac{1}{2}, \tag{A1}$$

$$\int_{-\infty}^{\infty} \zeta_2 \hat{k}_2^s(s, \Delta)\, d\Delta = 0, \tag{A2}$$

$$\int_{-\infty}^{\infty} \zeta_2 \hat{k}_4^s(s, \Delta)\, d\Delta = \frac{1}{2}. \tag{A3}$$

As an example we would like to demonstrate (41), where

$$\xi K_2^{(-1)} = \frac{1}{2\pi}\frac{(E-K)\xi^4 + (8E-6K)\xi^2}{(4+\xi^2)^{3/2}}, \tag{A4}$$

and $E = E(2/\sqrt{4+\xi^2})$, $K = K(2/\sqrt{4+\xi^2})$ are given in terms of the elliptic integrals

$$E(k) = \int_0^1 \frac{\sqrt{1-t^2k^2}}{\sqrt{1-t^2}}\,dt, \quad K(k) = \int_0^1 \frac{1}{\sqrt{1-t^2k^2}\sqrt{1-t^2}}\,dt. \tag{A5}$$

Expanding the integrands of the identities (A1)–(A3) in s using a uniform approximation as described in Sec. III, one obtains an infinite sequence of identities for the integral over the inner variable ξ, for each order in s. In this fashion, at order s^0 we find from (A2) that

$$I_2^{(s,0)} \equiv \int_{-\infty}^{\infty} \frac{(E-K)\xi^4 + (7E-5K)\xi^2 + 4E}{(4+\xi^2)^{3/2}}\,d\xi = 0,$$

and from (A1) at order s^{-1} that

$$I_1^{(s,-1)} \equiv \int_{-\infty}^{\infty} \frac{(K-E)\xi^2 + 4E}{(4+\xi^2)^{3/2}}\,d\xi = \pi.$$

Clearly,

$$2\pi \int_{-\infty}^{\infty} \xi K_2^{(-1)} d\xi = -I_1^{(s,-1)} + I_2^{(s,0)} = -\pi,$$

which is equivalent to (41). Other integrals over elliptic integrals, like (41) or (65), can be evaluated in a similar way.

The integral (63) is slightly different, in that it had to be made convergent by subtracting the asymptotic behavior $j_1^{(z)} \approx -1/(4\xi)$ for large ξ. Instead of using (A1)–(A3), we compute (63) directly. Expanding $\hat{j}_z$ in the inner variable ξ, we find that $j_1^{(z)} = -K/(2\pi\sqrt{4+\xi^2})$. Substituting $\zeta = 2/\sqrt{4+\xi^2}$, one can show that the integral in (63) is equivalent to

$$I_s \equiv \int_0^1 \left[\frac{1}{4} - \frac{K(\zeta)}{2\pi}\right]\frac{d\zeta}{\zeta\sqrt{1-\zeta^2}},$$

noting that

$$\int_0^{\infty} \left(\frac{1}{1+\xi} - \frac{1}{\sqrt{4+\xi^2}}\right) d\xi = 0.$$

With the definition (A5), we find

$$I_s = \frac{1}{2\pi}\int_0^1\int_0^1 \left(\frac{\sqrt{1-t^2\zeta^2}-1}{\sqrt{1-t^2}\sqrt{1-t^2\zeta^2}}\right)\frac{d\zeta\,dt}{\zeta\sqrt{1-\zeta^2}} = \frac{1}{4\pi}\int_0^1 \frac{\ln(1-t)+\ln(1+t)}{\sqrt{1-t^2}}\,dt = -\frac{\ln 2}{4},$$

using [51], 4.292, for the last identity.

APPENDIX B: INTEGRALS OVER THE ENTIRE DROP

To compute

$$\int_{\ln(2R)}^{l} \zeta_2 \overline{\kappa}\, \hat{j}_z^e\, dl_2,$$

which is the integral in (71), we develop a composite solution for $\zeta_2\overline{\kappa}\hat{j}_z^e$. Inserting (76) into (51) and (26), and expanding for large l, the inner part of the solution becomes

$$\zeta_2\overline{\kappa}\hat{j}_z^e\big|_{\text{in}} = -\frac{1}{4\sqrt{l}} + \frac{1}{4\sqrt{l}^3}\left[\frac{-l_0}{2} + 2 - \left(\frac{9}{8} - \frac{\ln 2}{2}\right)\ln l + \frac{\ln^2 l}{8}\right]. \tag{B1}$$

To compute the outer solution, note that

$$\hat{j}_z^e = -\frac{\overline{h}[\overline{h}'(2\xi^2 - \overline{h}^2) - \xi\overline{h}]}{4(\xi^2 + \overline{h}^2)^{3/2}}, \quad \kappa = \frac{1}{\overline{h}(1+\overline{h}'^2)^{1/2}} - \frac{\overline{h}''}{(1+\overline{h}'^2)^{3/2}},$$

so using (83) and expanding in ϵ, we obtain

$$\overline{\kappa}\hat{j}_z^e\big|_{\text{out}} = \frac{\epsilon}{4\xi^2}[h_0(\xi - 1) - 2h_0'(\xi - 1)\xi] + O(\epsilon^3) = \frac{\epsilon}{16\xi}(3\xi - 2) + O(\epsilon^3). \tag{B2}$$

It is seen from (100) that only terms up to order $(\ln R)^{-1/2}$ are needed, so it is enough to include terms of order ϵ in the inner solution. Finally, taking the limit $\xi \to 0$ in (B2) we find the solution in the overlap region:

$$\overline{\kappa}\hat{j}_z^e\big|_{\text{over}} = -\frac{\epsilon}{8\xi} + O(\epsilon^3), \tag{B3}$$

so that the composite solution is

$$\overline{\kappa}\hat{j}_z^e\big|_{\text{comp}} = \overline{\kappa}\hat{j}_z^e\big|_{\text{in}} + \overline{\kappa}\hat{j}_z^e\big|_{\text{out}} + \frac{\epsilon}{8\xi}, \tag{B4}$$

where ϵ is given in terms of $\ln R$ by (97). Combining the last two terms of (B4), the integral becomes convergent for $R \to \infty$ at the lower end, so we can approximate

$$\int_0^2 \left(\overline{\kappa}\hat{j}_z^e\Big|_{\text{out}} + \frac{\epsilon}{8\xi}\right)d\xi \approx \epsilon\int_0^2 \left(\frac{3\xi - 2}{16\xi} + \frac{\epsilon}{8\xi}\right)d\xi = \frac{3\epsilon}{8} \approx \frac{3}{4\sqrt{\ln R}}.$$

Further, performing the integral over (B1), we find

$$\int \zeta_2\overline{\kappa}\hat{j}_z^e\big|_{\text{in}} dl_2 = -\frac{\sqrt{l}}{2} + \left[\frac{l_0}{4} - \frac{3}{8} - \frac{\ln 2}{2} + \left(\frac{5}{16} - \frac{\ln 2}{4}\right)\ln l - \frac{\ln^2 l}{16}\right]\frac{1}{\sqrt{l}},$$

so that we obtain (101).

Next we come to the integrals in (66). To calculate the second integral, we note that the (z, z) component of (6) implies that

$$\int_{-\infty}^{\ln(2R)} \zeta_2 k_1\, dl_2 = \frac{1}{2}.$$

Thus separating the local contribution, the integral can be written as (up to exponentially small corrections):

$$\frac{1}{2} = \int_{-\infty}^{\infty} \left[\zeta_2\hat{k}_1 - H(\Delta)\zeta_2\hat{k}_1^e\right]dl_2 + \int_l^{\ln(2R)} \zeta_2\hat{k}_1^e\, dl_2 \equiv I_0 + I_1.$$

Computing the local integral I_0 in the usual way by expanding about a cone of slope $s(l)$ and using composite solutions, one finds that $I_0 = 1/2 - 3s^2/4 \approx 1/2 - 3/(4l)$, which means that I_1, which is the second integral in (66), is $I_1 = 3/(4l) + O(l^{-2})$.

To compute the first integral in (66), we need a composite description of the integrand $\zeta_2\hat{k}_1^e v_z(l_2)$, which in outer variables reads $\xi\overline{k}_1^e\overline{v}_z(l_2)/\epsilon$. We compute the inner version based on the inner solutions (76) and (77) and the outer version from (83) and (92). Taking the inner limit of the outer

solution, one confirms that the leading term as $\xi \to$ agrees with the leading term as $\ln(R) \to \infty$ of the inner solution, and the overlap is

$$\left.\frac{\xi \overline{k}_1^e \overline{v}_z}{\epsilon}\right|_{\rm over} = -\frac{3\epsilon^3}{64\xi} \approx -\frac{3}{64\xi(\ln R)^{3/2}}.$$

Writing the composite solution as

$$\zeta_2 k_1^e v_z \approx \zeta_2 k_1^e v_z\big|_{\rm in} + \left.\frac{\xi}{\epsilon}\overline{k}_1^e \overline{v}_z\right|_{\rm out} - \left.\frac{\xi}{\epsilon}\overline{k}_1^e \overline{v}_z\right|_{\rm over},$$

the integral becomes

$$\int_l^{\ln(2R)} \zeta_2 k_1^e v_z(l_2)\, dl_2 \approx \int_l^{\ln(2R)} \zeta_2 k_1^e v_z\big|_{\rm in} dl_2 + \frac{1}{\epsilon}\int_{e^l/R}^2 \big(\overline{k}_1^e \overline{v}_z\big|_{\rm out} - \overline{k}_1^e \overline{v}_z\big|_{\rm over}\big) d\xi.$$

The first integral is to leading order

$$\int_l^{\ln(2R)} \zeta_2 k_1^e v_z\big|_{\rm in} dl_2 \approx -\frac{3}{8}\int_l^{\ln(2R)} \frac{dl}{l^{3/2}} = \frac{3}{4}\left(\frac{1}{\sqrt{\ln 2R}} - \frac{1}{\sqrt{l}}\right) \approx \frac{3}{4}\left(\frac{1}{\sqrt{\ln R}} - \frac{1}{\sqrt{l}}\right),$$

and to leading order

$$\left.\frac{1}{\epsilon}\overline{k}_1^e \overline{v}_z\right|_{\rm out} = -\frac{3(\xi-2)(\xi-1)\epsilon}{32} \approx -\frac{3(\xi-2)(\xi-1)}{16\sqrt{\ln R}}.$$

The contribution from $\epsilon^{-1}\overline{k}_1^e \overline{v}_z|_{\rm over}$ is of order $(\ln R)^{-3/2}$ and does not need to be considered, so we are left with

$$\frac{1}{\epsilon}\int_{e^l/R}^2 \big(\overline{k}_1^e \overline{v}_z\big|_{\rm out} - \overline{k}_1^e \overline{v}_z\big|_{\rm over}\big) d\xi \approx -\frac{3}{16\sqrt{\ln R}}\int_0^2 (\xi-2)(\xi-1)\, d\xi = -\frac{1}{8\sqrt{\ln R}}.$$

Taking these results together, we finally have

$$K_1 \approx \int_l^{\ln(2R)} \zeta_2 k_1^e v_z(l_2)\, dl_2 - \frac{3}{4l}\left(-\frac{\sqrt{l}}{2}\right) \approx \frac{3}{4}\left(\frac{1}{\sqrt{\ln R}} - \frac{1}{\sqrt{l}}\right) - \frac{1}{8\sqrt{\ln R}} + \frac{3}{8\sqrt{l}},$$

which means that we can identify the constant $C(R)$ to be (102).

[1] A. Prosperetti and G. Tryggvason, Introduction: A computational approach to multiphase flow, in *Computational Methods for Multiphase Flow*, edited by A. Prosperetti and G. Tryggvason (Cambridge University Press, Cambridge, 2007).

[2] A. T. S. Cerdeira, J. B. L. Campos, J. M. Miranda, and J. D. P. Araújo, Review on microbubbles and microdroplets flowing through microfluidic geometrical elements, Micromachines **11**, 201 (2020).

[3] G. I. Taylor, The formation of emulsions in definable fields of flow, Proc. R. Soc. London A **146**, 501 (1934).

[4] S. Courrech du Pont and J. Eggers, Sink Flow Deforms the Interface between a Viscous Liquid and Air into a Tip Singularity, Phys. Rev. Lett. **96**, 034501 (2006).

[5] M. Manga and H. A. Stone, Buoyancy-driven interactions between two deformable viscous drops, J. Fluid Mech. **256**, 647 (1993).

[6] G. I. Taylor, Conical free surfaces and fluid interfaces, in *Proceedings of the 11th International Congress of Applied Mathematics, Munich (Germany)*, edited by H. Görtler (Springer, Heidelberg, 1964), pp. 790–796.

[7] J. D. Buckmaster, Pointed bubbles in slow viscous flow, J. Fluid Mech. **55**, 385 (1972).

[8] J. D. Buckmaster, The bursting of pointed drops in slow viscous flow, J. Appl. Mech. **40**, 18 (1973).

[9] A. Acrivos and T. S. Lo, Deformation and breakup of a single slender drop in an extensional flow, J. Fluid Mech. **86**, 641 (1978).
[10] E. J. Hinch and A. Acrivos, Steady long slender droplets in two-dimensional straining motion, J. Fluid Mech. **91**, 401 (1979).
[11] G. K. Youngren and A. Acrivos, On the shape of a gas bubble in a viscous extensional flow, J. Fluid Mech. **76**, 433 (1976).
[12] J. M. Rallison, The deformation of small viscous drops and bubbles in shear flows, Annu. Rev. Fluid Mech. **16**, 45 (1984).
[13] B. J. Bentley and L. G. Leal, A computer-controlled four-roll mill for investigations of particle and drop dynamics in two-dimensional linear shear flows, J. Fluid Mech. **167**, 219 (1986).
[14] B. J. Bentley and L. G. Leal, An experimental investigation of drop deformation and breakup in steady, two-dimensional linear flows, J. Fluid Mech. **167**, 241 (1986).
[15] J. Eggers and S. Courrech du Pont, Numerical analysis of tip singularities in viscous flow, Phys. Rev. E **79**, 066311 (2009).
[16] J. P. K. Tillett, Axial and transverse Stokes flow past slender axisymmetric bodies, J. Fluid Mech. **44**, 401 (1970).
[17] H. Ashley and M. Landahl, *Aerodynamics of Wings and Bodies* (Addison-Wesley, Reading, MA, 1965).
[18] J. N. Newman, Applications of slender-body theory in ship hydrodynamics, Annu. Rev. Fluid. Mech. **2**, 67 (1970).
[19] E. O. Tuck and Y. M. Stokes, On thin or slender bodies, ANZIAM J. **53**, 190 (2012).
[20] D. Bonn, J. Eggers, J. Indekeu, J. Meunier, and E. Rolley, Wetting and spreading, Rev. Mod. Phys. **81**, 739 (2009).
[21] S. L. Anna, Droplets and bubbles in microfluidic devices, Annu. Rev. Fluid Mech. **48**, 285 (2016).
[22] J. Dong, M. Meissner, J. Eggers, A. M. Seddon, and C. P. Royall, Opposed flow focusing: Evidence of a second order jetting transition, Soft Matter **14**, 8344 (2018).
[23] R. Suryo and O. A. Basaran, Tip streaming from a liquid drop forming from a tube in a co-flowing outer liquid, Phys. Fluids **18**, 082102 (2006).
[24] A. M. Gañán-Calvo, R. González-Prieto, P. Riesco-Chueca, M. A. Herrada, and M. Flores-Mosquera, Focusing capillary jets close to the continuum limit, Nat. Phys. **3**, 737 (2007).
[25] W. W. Zhang, Viscous Entrainment from a Nozzle: Singular Liquid Spouts, Phys. Rev. Lett. **93**, 184502 (2004).
[26] E. Castro-Hernández, F. Campo-Cortés, and J. M. Gordillo, Slender-body theory for the generation of micrometre-sized emulsions through tip streaming, J. Fluid Mech. **698**, 423 (2012).
[27] I. Cohen and S. R. Nagel, Scaling at the Selective Withdrawal Transition through a Tube Suspended Above the Fluid Surface, Phys. Rev. Lett. **88**, 074501 (2002).
[28] S. C. Case and S. R. Nagel, Spout States in the Selective Withdrawal of Immiscible Fluids Through a Nozzle Suspended Above a Two-Fluid Interface, Phys. Rev. Lett. **98**, 114501 (2007).
[29] S. Courrech du Pont and J. Eggers, Fluid interfaces with very sharp tips in viscous flow, Proc. Natl. Acad. U. S. A. **117**, 32238 (2020).
[30] S. Richardson, Two-dimensional bubbles in slow viscous flows, J. Fluid Mech. **33**, 476 (1968).
[31] J.-T. Jeong and H. K. Moffatt, Free-surface cusps associated with a flow at low Reynolds numbers, J. Fluid Mech. **241**, 1 (1992).
[32] J. Eggers, Air Entrainment through Free-Surface Cusps, Phys. Rev. Lett. **86**, 4290 (2001).
[33] É. Lorenceau, F. Restagno, and D. Quéré, Fracture of a Viscous Liquid, Phys. Rev. Lett. **90**, 184501 (2003).
[34] S. D. Howison and S. Richardson, Cusp development in free boundaries, and two-dimensional slow viscous flows, Eur. J. Appl. Math. **6**, 441 (1995).
[35] L. K. Antanovskii, Formation of a pointed drop in Taylor's four-roller mill, J. Fluid Mech. **327**, 325 (1996).
[36] C. Pozrikidis, *Boundary Integral and Singularity Methods for Linearized Flow* (Cambridge University Press, Cambridge, 1992).

[37] J. M. Rallison and A. Acrivos, A numerical study of the deformation and burst of a viscous drop in an extensional flow, J. Fluid Mech. **89**, 191 (1978).
[38] P. Doshi, I. Cohen, W. W. Zhang, M. Siegel, P. Howell, O. A. Basaran, and S. R. Nagel, Persistence of memory in drop breakup: The breakdown of universality, Science **302**, 1185 (2003).
[39] J. Eggers and M. A. Fontelos, *Singularities: Formation, Structure, and Propagation* (Cambridge University Press, Cambridge, 2015).
[40] I. Cohen, M. P. Brenner, J. Eggers, and S. R. Nagel, Two Fluid Drop Snap-Off Problem: Experiment and Theory, Phys. Rev. Lett. **83**, 1147 (1999).
[41] A. Sierou and J. R. Lister, Self-similar solutions for viscous capillary pinch-off, J. Fluid Mech. **497**, 381 (2003).
[42] M. Van Dyke, *Perturbation Methods in Fluid Mechanics* (Parabolic Press, Stanford, CA, 1975).
[43] E. J. Hinch, *Perturbation Methods* (Cambridge University Press, Cambridge, 1991).
[44] G. Huisken, Local and global behaviour of hypersurfaces moving by mean curvature, Proc. Symposia Pure Math. **54**, 175 (1993).
[45] S. B. Angenent and J. J. L. Velázquez, Degenerate neckpinches in mean curvature flow, J. für Reine und Angew. Math. **482**, 15 (1997).
[46] J. Eggers and M. A. Fontelos, The role of self-similarity in singularities of partial differential equations, Nonlinearity **22**, R1 (2009).
[47] J. Eggers, M. A. Fontelos, D. Leppinen, and J. H. Snoeijer, Theory of the Collapsing Axisymmetric Cavity, Phys. Rev. Lett. **98**, 094502 (2007).
[48] J. M. Gordillo, A. Sevilla, and F. Campo-Cortés, Global stability of stretched jets: Conditions for the generation of monodisperse micro-emulsions using coflows, J. Fluid Mech. **738**, 335 (2014).
[49] A. Evangelio, F. Campo-Cortés, and J. M. Gordillo, Simple and double microemulsions via the capillary breakup of highly stretched liquid jets, J. Fluid Mech. **804**, 550 (2016).
[50] K. He, F. Campo-Cortés, M. Goral, T. López-Léon, and J. M. Gordillo, Micron-sized double emulsions and nematic shells generated via tip streaming, Phys. Rev. Fluids **4**, 124201 (2019).
[51] I. S. Gradshteyn and I. M. Ryzhik, *Table of Integrals Series and Products* (Academic, New York, 2014).